B. TECH. PROJECT REPORT

On

Surface Modification of Aluminium Alloy

BY

Tirthesh Ingale, (160005016)
Manish Kumar, (160005018)

DISCIPLINE OF METALLURGY ENGINEERING & MATERIALS SCIENCE
INDIAN INSTITUTE OF TECHNOLOGY INDORE

December 2019

Surface Modification of Aluminium Alloy

A PROJECT REPORT

Submitted in partial fulfillment of the requirements for the award of the degrees

of
BACHELOR OF TECHNOLOGY
in

METALLURGY ENGINEERING AND MATERIALS SCIENCE

Submitted by:
Tirthesh Ingale, (160005016)
Manish Kumar, (160005018)

Guided by:
Dr. Santosh S. Hosmani,
Associate Professor, IIT Indore.

INDIAN INSTITUTE OF TECHNOLOGY INDORE
December 2019

CANDIDATE'S DECLARATION

We hereby declare that the project entitled **"Surface Modification of Aluminium Alloy"** submitted in partial fulfillment for the award of the degree of Bachelor of Technology in 'Metallurgy Engineering and Materials Science' completed under the supervision of **Dr. Santosh S. Hosmani (Associate Professor),** IIT Indore is an authentic work.

Further, we declare that we have not submitted this work for the award of any other degree elsewhere.

Signature and name of the student(s) with date

Tirthesh Ingale (160005016) **Manish Kumar (160005018)**

CERTIFICATE by BTP Guide

It is certified that the above statement made by the students is correct to the best of my knowledge.

Signature of BTP Guide with dates and their designation

Dr. Santosh S. Hosmani,

Associate Professor, IIT Indore.

Preface

This report on “Surface Modification of Aluminium Alloy" is prepared under the guidance of Dr. Santosh S. Hosmani.

Through this report we have tried to give detailed experimental information about surface modification techniques of aluminium like Friction Stir Processing, Surface Texturing, Surface Mechanical Attrition Treatment and Anodizing.

We have tried to the best of our abilities and knowledge to explain the content in a lucid manner. We have also added Micrographs and figures to make it more illustrative.

Tirthesh Ingale (160005016) and Manish Kumar (160005018)
B.Tech. IV Year,
Discipline of Metallurgy Engineering and Materials Science,
IIT Indore.

Acknowledgments

I express my deep sense of gratitude to the Almighty for guiding me and giving patience throughout this duration. Inspiration and guidance are valuable in all aspects of life. This venture has received the hearty support of my Supervisor **Dr. Santosh S. Hosmani**. Constant encouragement, motivation, and enthusiasm from my guide helped me to move forward with an investigation in depth. I take this opportunity to express my profound gratitude to **Prof. Pradeep Mathur,** Director, IIT Indore for providing the essential facilities, valuable guidance and cooperation.

We also want to thank **Discipline of Metallurgy Engineering & Material Science, IIT Indore** for the funding of experimental expenses and allowing us to use the material lab equipments for our experiments. Without their support, this report would not have been possible.

Last but not least, I cannot forget the support and encouragement received from **Mr. Manoj D. Joshi, Mr. Digvijay Singh, Mr. Aditya Litoria, Mr.Vikesh Kumar** (PhD research scholars) and **Mr. Mayur Dhake** without which this journey would not have been possible.

Tirthesh Ingale (160005016) and Manish Kumar (160005018)
B.Tech. IV Year,
Discipline of Metallurgy Engineering and Materials Science,
IIT Indore.

IV

Abstract

In the present work, mechanical and surface (tribological) properties of Aluminium alloy are modified using various surface modification techniques like Friction Stir Processing (FSP), Surface texturing, Surface Mechanical Attrition Treatment (SMAT) and Anodizing. Improvement in the hardness of Aluminium alloy was achieved by fabricating Aluminium metal matrix composite with ZrO_2 reinforcement using FSP. In post-FSP T6 heat-treatment, aging kinetics was observed. It was effective in achieving 95% more surface hardness than non FSPed specimen. The surface textures of depths 50, 100 and 150 μm were created on aluminium 6060 specimens using Wire Electrical Discharge Machine (WEDM). Surface Mechanical Attrition Treatment was another method used for surface modification. Moving bearing balls were subjected towards aluminium surface for Severe Plastic Deformation. It provided grain refinement and hence improvement in hardness. Textured and SMATed specimens further modified using Al_2O_3 coating (Anodizing). Sliding wear test showed increment in wear resistance by using SMAT and anodizing under both dry and lubricated wear conditions. Under the lubricated condition, SMATed specimen showed 4 times lower wear loss in case of non-anodized specimens while Al_2O_3 coating over SMATed specimen showed a further reduction in wear loss about 16 times lower than that of non processed specimen. Textured and SMATed specimens showed improvement in COF under lubricated condition. Lowest 0.02 COF was achieved for Non-Textured Anodized specimen. These results indicate the effectiveness of FSP, texturing and SMAT in surface modification of aluminium alloy.

Table of Contents

List of Figures

List of Tables

Nomenclature

List of Abbreviations and Symbols

SPD	Severe Plastic Deformation
FSP	Friction Stir Processing
SMAT	Surface Mechanical Attrition Treatment
CNC	Computer Numerical Control
WEDM	Wire cut Electrical Discharge Machining
XRD	X-Ray Diffraction
Ø	Diameter
T.M.Z.	Thermo-Mechanically Affected Zone
S.Z.	Stirred Zone
B.M.	Base Metal
Ɵ	Incident Angle
SEM	Scanning Electron Microscope
COF	Coefficient of Friction
FCC	Face Centred Cubic

Chapter 1

Introduction

Many engineering applications demand lightweight components to enhance their efficiency and economy. But, these components should not be compromised with their strength when compared to other globally accepted industrial materials like steel. Aluminium alloys are one of the attractive engineering materials for their better machinability and lower density compared to steels. However they are soft materials and have poor mechanical properties. Surface modifications are required for improving performance of aluminium alloys. Grain refinement, surface micro-texturing and surface coatings are workable surface modification techniques for enhancing properties of aluminium alloys [1-3].

In order to enhance the mechanical strength of aluminium and its alloys, various surface modification treatments are performed. Conventional surface modification techniques such as laser melt treatment, plasma spraying, and liquid phase processing techniques etc. are performed at elevated temperatures, which could possibly result in the formation of unwanted brittle phases during solidification. To eliminate the adverse effects of liquid state processing, solid-state processing proved to be one of the effective alternatives to enhance the properties of light metal alloys. These processes limit the material distortion and residual stress generation which in turn improves the mechanical strength of the material [4].

Compared to other strengthening techniques Grain refinement can deliver combination of ultrahigh strength as well as ductility which is required for ambient and cryogenic temperature applications [4]. Broad research is being undertaken to further improve Severe Plastic Deformation (SPD) techniques, which can produce ultra-fine grained metals and alloys commercially. Friction Stir Processing (FSP) is one of the solid state SPD techniques which can generates vast shear strain into the material and thereby produces ultra-fine grain structure of the submicron level. The approach of fabrication of surface composite using FSP can help in achieving the good surface hardness and wear resistance without compromising the original properties of the substrate [5]. FSP possess many advantages over conventional routes of processing which include lack of casting defects, uniform distribution of alloying elements and reinforcements (in case of composites), phase homogenization, etc. [6, 7].

Friction stir processing is basically a local thermo-mechanical metalworking method, wherein, a rotating tool having a pin and shoulder is plunged into a work piece that alters the localized microstructure. It provides plastic flow by frictional heat and stirring, thereby refining the microstructure of the material and dispersion of reinforcements in metals and alloys in order to manufacture composites [5]. Material mixing in the stirred zone is considerably dependent on the geometry of the rotating tool [8]. The triangular and square pin tools produce a pulsating stirring action in the flowing material (due to their flat faces). However, there is no such pulsating action in case of cylindrical, tapered and threaded pin profiles [8].

M. Sivanesh Prabhu et al. [9] obtained increment in hardness and wear resistance due to FSP. H.A. Deore, J. Mishra et al. [10] and Kaustubh M. Mane et al. [11] obtained further increment in hardness after post processing aging heat treatment. An optimum combination of transverse speed and a rotational speed of the tool is essential to achieve the maximum hardness of the surface composites [5].

In the manufacturing of materials, wear system design is a very important criterion requiring consideration which ensures the reliability of the material in applications where they come in contact with the environment and other surfaces. Wear is one of the most frequently encountered industrial issues where the material is affected mainly by speed, environmental conditions, and working load [12]. Wear is a slow and progressive loss of materials which are subjected to repeated rubbing action, which causes an enormous amount of expenditure by repairing or replacing the worn-out parts or equipment [13]. So, many research works has been going on for improvement of tribological properties of metal and alloys.

The addition of surface texture to the solid surface enables the control of tribological behaviour [13, 14]. Surface texturing is the intentional introduction of well-defined identical features (discrete dimples, grooves) on surfaces. It provides several benefits such as micro-textures act as lubricant reservoir, it also provide secondary lubrication during sliding wear [14]. During boundary lubrication load carrying capacity can be improved by using micro-textures. Micro-textures also show entrapment of third body abrasives [15]. However, it has a limitation that it worn out easily at the contact of texture.

Surface mechanical attrition treatment (SMAT) is also one of the solid state processes in which the surface of the metals is subjected to severe plastic deformation using the impacts of randomly moving balls. These moving balls impact the projected specimen surface to induce the accumulative strain, which results in the grain refinement of the treated surface [16]. This provides the enhancement of several properties, like surface hardness, wear resistance, yield strength and ultimate tensile strength [16, 17]. Xiangchen Meng et al [1] and Yong Liu et al [18] observed grain refinement up to nanostructured grains after SMAT of Aluminium. They observed improved mechanical properties due to severe plastic deformation by SMAT.

The single surface treatment is unable to show effective tribological performance. Production of porous Anodic Aluminium Oxide layer can deal with this problem. This can be achieved by using anodizing technique. Anodizing is the surface coating of aluminium using Al_2O_3 oxide layer. Strong Al_2O_3 layer on aluminium surface improves its wear resistance [3]. Luanxia Chen et al [19] have found improved tribological performance of aluminium by anodizing of textured surfaces with the help of MoS_2 coatings. There is a lack of literature regarding anodizing of textured and SMATed aluminium alloys.

In the present work, various surface modification techniques are studied.

1. ZrO_2 powder is mechanically mixed on the surface of Al 6060 alloy using Friction Stir Process (FSP).
2. Texturing of aluminium surface using WEDM.
3. SMAT of aluminium 6060 surface.
4. Anodizing of textured and SMATed aluminium 6060.

Influence of these surface modification techniques on properties of aluminium 6060 alloy are studied in this work.

Chapter 2

Objectives

- To study influence of surface modification on the surface properties of aluminium alloys using various techniques.
- To fabricate Aluminum metal matrix composite using Friction Stir Processing.
- To study the influence of Friction Stir Processing on mechanical and tribological properties of Aluminum alloy.
- To study the effect of surface texturing on tribological behavior of aluminium surface under dry and lubricated condition.
- To study the influence of Surface Mechanical Attrition Treatment on mechanical and tribological properties of aluminium surface.
- Anodizing of textured and SMATed specimens.
- Effect of anodizing on aluminium 6060 alloy.
- Influence of anodizing on tribological properties of textured and SMATed specimens.

Chapter 3

Experimental Methodology

In this work, Al 6060 was selected as the substrate for FSP and texturing. This alloy is a heat treatable grade of Al alloys. The chemical composition of this alloy is shown in Table 1. For FSP, circular plates of 8mm thickness and 90mm diameter were cut from a cylinder. These samples were subjected to stress-relieving annealing heat treatment at 420°C for 2 hours followed by furnace cooling.

Table 1 Chemical composition of as received Al 6060 alloy

Element	Al	Si	Mg	Fe	Mn	Ti	Zn	Cr
Weight %	98.71	0.48	0.47	0.19	0.096	0.028	0.018	0.014

Two different geometries of the tool were used for FSP: (1) square pin and (2) pinless tools as shown in Fig. 1. Shoulder and shank diameter was 15 and 14 mm respectively for both the tools. Shank helped to hold the tool in collet during processing on the CNC (computer numerical control) machine. The dimension of square pin sides was 6 mm and the length of the pin was 1 mm. EN31 tool steel (High Carbon High Chromium-HCHCr) material was used for tool manufacturing.

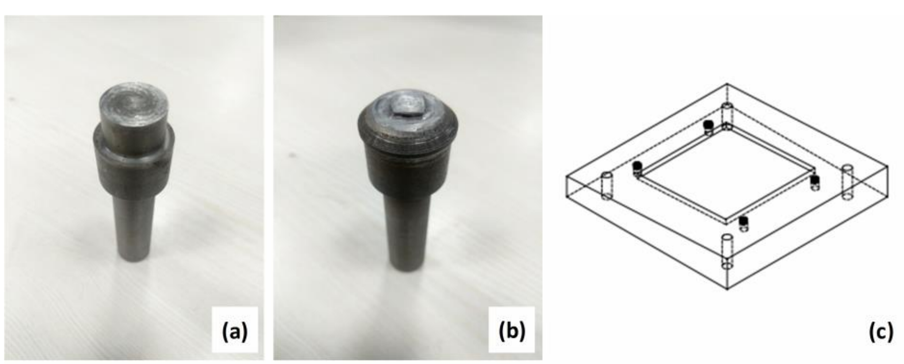

Fig. 1(a) Pinless Tool, (b) Tool with square pin, (c) Fixture with 3° tapered arrangement

FSP was done on the Vertical Milling Machine. All the degrees of freedom of the specimen during friction stir processing were restricted using the fixture. During FSP, traversing and rotating tool must tilt towards the trailing side of the traversing direction to ensure proper forging action on the specimen and mixing/stirring of material [11]. Generally, this tilt angle could be provided by tilting the spindle of the machine. As this facility was not available in the machine used in this work, an alternative arrangement was made to provide the tilt angle. A plate with 3° gradient was designed for this purpose. Al 6060 specimen was kept on this gradient plate and clamped to the fixture plate. The CNC programming was done such that the tool traversed horizontally and vertically simultaneously (to move along the gradient plate), and thus, maintained the constant plunge depth throughout the scan.

Firstly, a groove was made on the base materials using WEDM with depth and width of 1mm and 3mm, respectively. The grooves were completely filled with Zirconia powder and then was closed using a tool comprising only of a shoulder and no pin (pinless tool). This was used to avoid ejecting powder out of the groove during the process. After this, the specimen was FSPed using square pin tool using 3° tilt angle. According to the literature, more rotation speed and less traverse speed provides better defect-free processing. So, 3000 rpm and 10 m/s traverse speed were chosen [11]. Three passes were carried out for obtaining proper mixing and more grain refinement [20]. One specimen was processed only with square pin tool without filling any powder for studying the effect of only stirring and grain refinement.

FSP specimens were subjected to T6 heat treatment for the study of artificial aging. T6 heat treatment involved solutionizing at 530 °C for 2 hours (followed by water quenching). Artificial aging was done at 175 °C for 8 hours (shown in Fig. 2) [11].

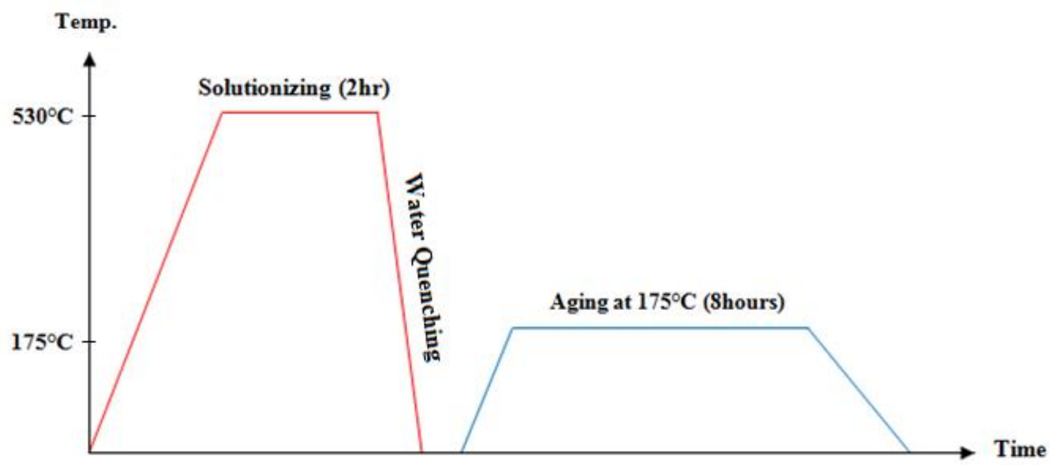

Fig. 2 T6 Heat Treatment cycle.

One as-received specimen was FSPed using Zirconia powder. Al-ZrO_2 shows aging effect at 377°C, so aging was carried out at 377 °C for 24 hours [21]. Designations of all FSP specimens are shown in Table 2.

Table 2 Designations of specimens of FSP.

Sr. No.	Long Name	Designation
1.	As Received	AR
2.	As Received - FSPed with ZrO_2	AR-FSPZrO_2
3.	As Received - FSPed with ZrO_2 - Heat Treated	AR-FSPZrO_2-HT
4.	As Annealed	AA
5.	As Annealed - FSPed without ZrO_2	AA-FSP
6.	As Annealed - FSPed without ZrO_2 - Heat Treated	AA-FSP-HT
7.	As Annealed - FSPed with ZrO_2	AA-FSPZrO_2
8.	As Annealed - FSPed with ZrO_2 - Heat Treated	AA-FSPZrO_2-HT

Microstructures of the polished and etched (Modified Tucker's reagent composition is shown in Table 3) specimens were obtained using an optical microscope (Make: Zeiss, Axio, Vert.A1). The hardness of the specimens was obtained using Brinell hardness tester (Make: Samarth Engineering, SE-B3000 P

C). Hardness measurements were carried out using 250 kgf load and 12 s dwell-time. Phases are examined using the X-Ray Diffraction (XRD, Make: Bruker D2-Phaser) method by Cu-Kα radiation with 1.54 Å wavelength from a diffraction angle 10–80°. XRD peaks were identified using XPERT-PRO XRD software.

Table 3 Composition of modified Tucker's Reagent

Compound	HF	HNO_3	HCl	H_2O
Proportion (in ml)	10	10	28	152

Wear tests were performed on ball-on-disk (Make: Magnum Engineers, TE-165) setup under dry conditions. Reciprocating wear was carried out using 10N load and 3Hz frequency for 20mm track radius with 20° angle. These tests were carried out for 20min under above loading conditions. Bearing ball made up of hardened steel with 62HRC hardness and 10mm size was used as counter body for wear tests. Specific wear rate was calculated by using weight loss method. Weight of the specimens before and after wear test was measured by using weighing machine with accuracy up to 0.01mg.

$$\text{Wear Rate} = \frac{Weight\ Loss\ (mg)}{Total\ distance\ covered\ (m)}$$

For texturing and SMAT, specimens of 6mm thickness and 70mm diameter were cut from cylindrical rods. Homogenization is carried out by subjecting these plates to solutionizing heat treatment at 530 °C for 2 hours followed by water quenching.

Surface texturing was carried out by using Wire cut Electrical Discharge Machining (WEDM). Grooves of equal width are created by keeping constant distance of 2.5 mm between two consecutive grooves. Initially parallel grooves are made. Then specimen is rotated through 90° and again parallel grooves were cut such that both the grooves are perpendicular to each other as shown in Fig. 3. Depths of the grooves are taken as 50, 100 and 150 μm.

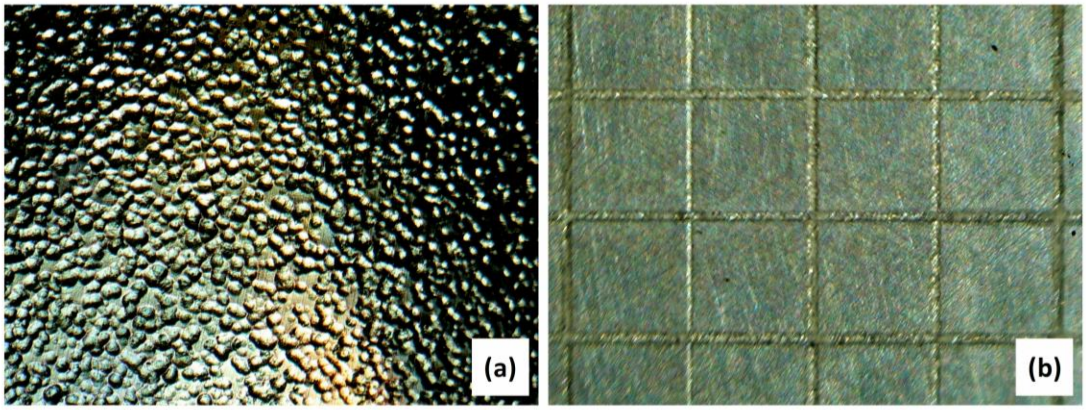

Fig. 3 (a) Macrograph of textured surface by WEDM, (b) Macrograph of top surface of SMATed region.

SMAT of the specimens was performed using in-house SMAT setup [16, 21]. Vibrational frequency of 100Hz was given to cylindrical SMAT cabin (ø 90 mm). 6mm bearing steel balls with hardness 62 HRC were used for the SMAT. SMAT was done for 30 min.

Anodizing coating was carried out over some SMATed and textured specimens. For the purpose of anodizing, specimens were cleaned initially with caustic soda solution followed by nitric cleaning. After cleaning, specimens are anodized in anodizing bath containing sulphuric acid and water in 3:7 ratio. Anodizing was carried out at 25 °C by supplying 12V voltage for 30 minutes. Thickness of 17.5 μm Al_2O_3 coating was obtained after anodizing process (Fig. 4). Presence of Al_2O_3 after anodizing was confirmed by X-Ray Diffraction method. Designations of all FSP specimens are shown in Table 4.

Table 4 Designations of specimens of texturing, SMAT and anodizing.

Sr. No.	Long Name	Designation
1.	As Homogenized	AH
2.	Textured using WEDM - 100 μm	T100
3.	Textured using WEDM - 150 μm	T150
4.	SMATed	SMAT
5.	As Homogenized + Anodized	AH-A
6.	Textured using WEDM - 50 μm + Anodized	T50-A
7.	Textured using WEDM - 100 μm + Anodized	T100-A
8.	SMATed + Anodized	SMAT-A

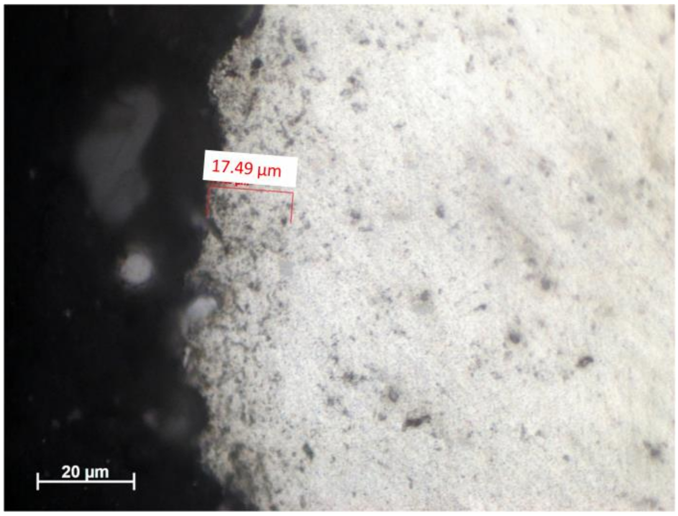

Fig. 4 Cross section of anodized specimen

2D profiles of these specimens were observed by using 2D surface profilometer (Make: Taylor and Hobson, 315). Hardness of the specimens was measured by using Brinell hardness tester. Hardness measurements were carried out using 5mm ball indenter, 250 kgf load and 12s dwell-time. Sliding wear tests were performed on a ball-on-disk tribometer under both dry and lubricated conditions (Fig. 5). Sliding tests were conducted at room temperature with the use of 20W40 engine oil as the lubricant. 8mm ball of hardened steel having 62 HRC was used as a counter body. Wear tests were taken under loading condition of 10N for 1000 m sliding distance with a sliding velocity of 0.25 m/s. Specific wear rates are calculated by using volume loss method. Initially area wore by wear test was measured by using 2D profilometer. Volume losses are calculated by using formula,

$$\text{Volume Loss} = \text{Wore area} \times 2\pi r$$

$$\text{Specific Wear Rate} = \frac{\mathit{Volume\ Loss}}{\mathit{Applied\ Load} \times \mathit{Total\ distance\ covered}}$$

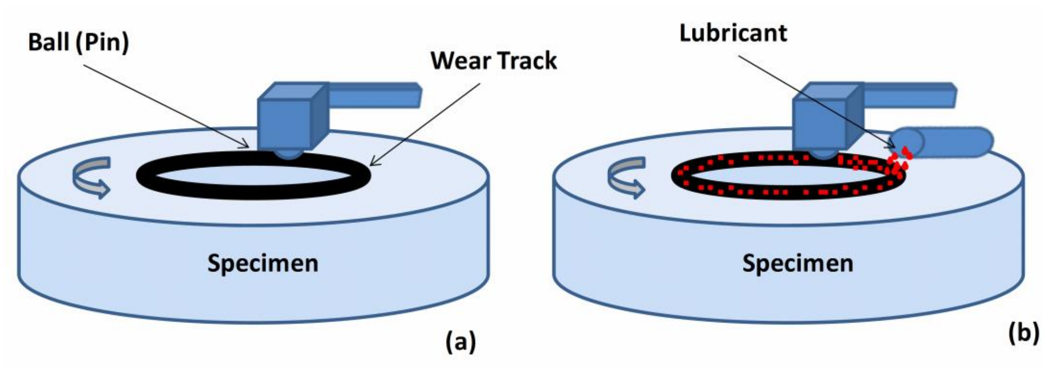

Fig. 5 Wear process under dry and lubricated conditions.

Chapter 4

Result and Discussion

4.1 Friction Stir Processing

4.1.1 Macro- and Micro-structural Analysis

Fig. 6 shows the top and cross-sectional macrographs of FSPed samples. Due to the combined effect of thermo-mechanical action, various zones are formed in FSPed specimen (Fig. 7) [11]. These zones are: (1) Base Metal (B.M.), (2) Thermo-Mechanically Affected Zone (T.M.Z.) and (3) Stirred Zone (S.Z.). Fig 6 shows micrographs of different zones.

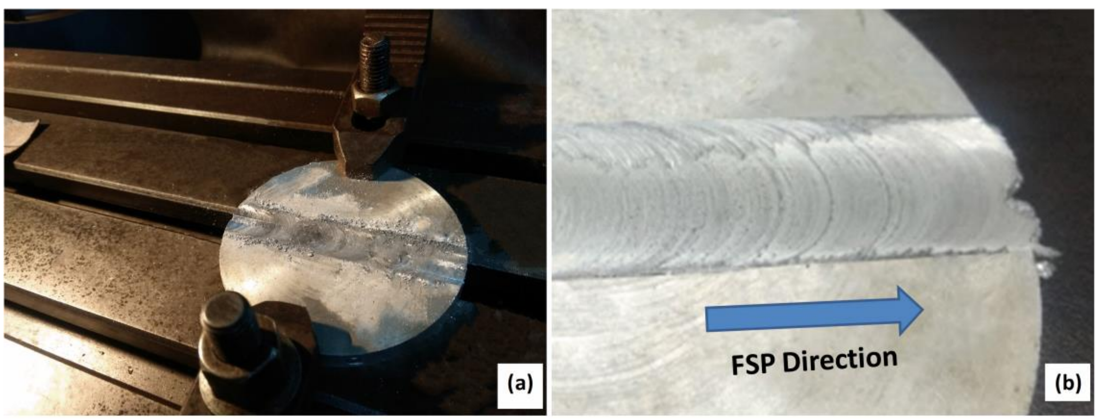

Fig. 6 (a) Macrographs after use of the pinless tool, (b) Macrograph after FSP with a square pin tool

Considerable grain refinement is observed in the stirred zone as compared to the base metal. It is due to severe plastic deformation and heat effect in FSPed region [9]. There being dynamic recrystallization leading to nucleation of new grains, restraining grain boundary sliding (GBS) and encouraging finer grain size [11]. An intermediate region of Thermo-Mechanically Affected Zone is observed in FSPed specimens. This zone experiences partial plastic deformation and lesser strain level relative to the stirred zone, but despite stirring, it did not undergo recrystallization [11]. Also, grains in (b) are finer than that in (d) due to thermo-mechanical action [22]. Zone away from FSPed region (B.M.) remained unaffected.

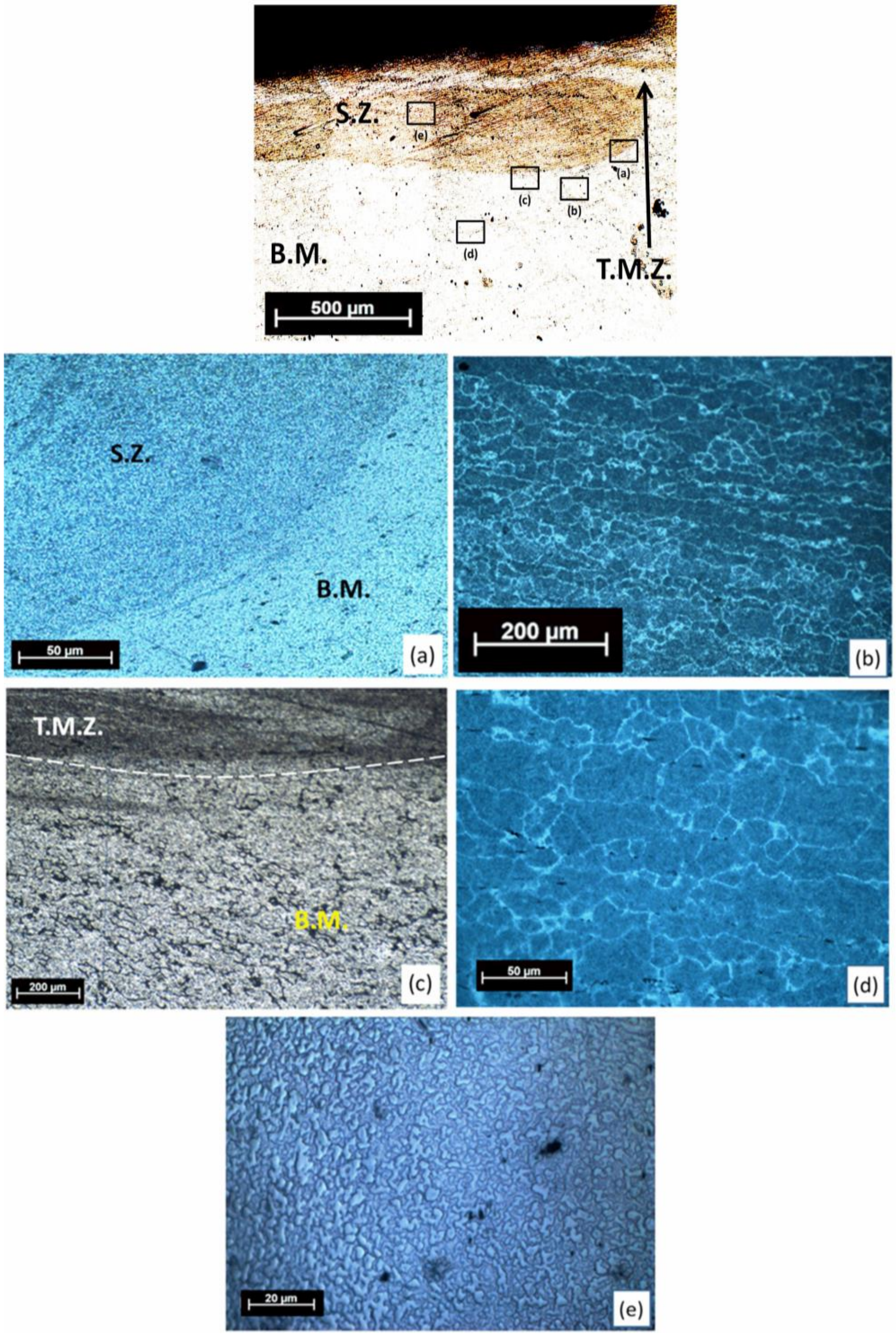

Fig. 7 Top of the figure shows the macrograph of the cross-section of the FSPed region of Al 6060. a–e are Micrographs of the various regions marked and labelled on the macrograph.

4.1.2 Hardness

Hardness measurements are taken for Friction Stir Processed specimens to understand the behaviour of FSP as well as heat treatment. Hardness comparison is shown in Fig. 8 for three different FSP conditions.

(1) FSP of stress relieved (annealed) aluminium using ZrO_2.

(2) FSP of stress relieved (annealed) aluminium without using ZrO_2.

(3) FSP of as received aluminium using ZrO_2.

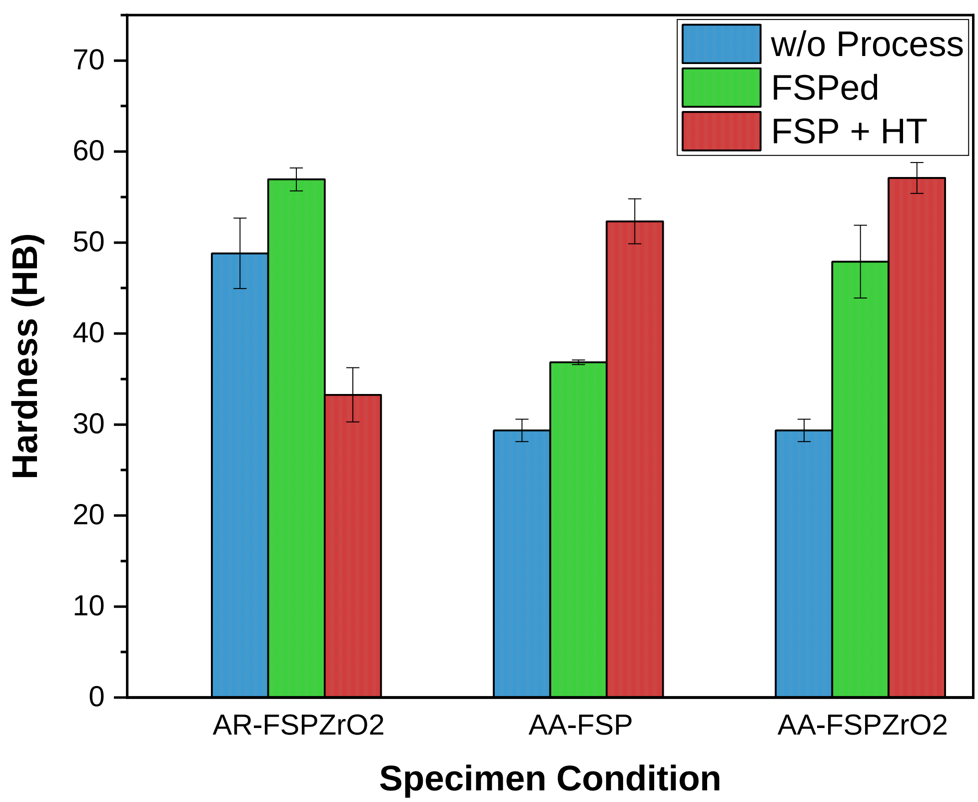

Fig. 8 Surface Hardness of FSPed aluminium specimens - without FSP, FSPed, FSP + HT.

AR aluminium had a hardness of 48.81 HB. After the FSP, there was a considerable increase in hardness after FSP. This increase in hardness is due to grain refinement [10, 11]. More dislocation pile-ups occur due to fine grains which result in an increase in hardness. Pedro Henrique Lamarao Souzaa et al [23] had shown that Al-Zr alloy gives best aging effects when aged at 377 °C. But in our case, FSPed specimens when aged at 377 °C for 24 hours resulted in a decrease in hardness. There may be two possible reasons behind the decrease in hardness. If as received samples are already deformed during its manufacturing, initially it may have some residual stresses. So, during aging it may get annealing heat treatment which reduces internal strain and hence decreases hardness [24]. Another possible reason is precipitation hardening by Si, Mg (already present in metal) and ZrO_2. Si, Mg gets peak aging within 8-10 hours [11]. So there is a possibility of over aging of Si and Mg precipitates when aged at 377 °C for 24 hours. If the contribution of Si and Mg (in case of magnitude) in precipitation hardening is more than that of ZrO_2, then decrease in hardness may be due to over aging of Si and Mg irrespective of aging of ZrO_2.

To avoid these negative effects, as received samples were stress relieved (annealed at 420 °C for 2 hours followed by furnace cooling) before processing. After this stress relieving heat treatment hardness of aluminium samples was 29.35HB. One of these specimens was FSPed by using ZrO_2 while another was FSPed without using ZrO_2. Due to grain refinement and higher dislocation density after FSP, there was an increase in hardness of both specimens [20]. The hardness of AA-FSP specimen was 36.84HB while that of specimen AA-FSP-ZrO_2 have hardness of 47.9HB. More hardness of Al-ZrO_2 composite than grain refined AA-FSP specimen is due to the presence of hard reinforcing ZrO_2 precipitates [20].

Aging effect was studied after T6 heat treatment of FSPed specimens. Considerable hardness increment was observed in both specimens. The hardness by AA-FSP-HT specimen increased up to 52.33HB, while that of AA-FSP-ZrO_2-HT specimen achieved hardness up to 57.1 after aging. This confirms that FSP with ZrO_2 helps in enhancing surface hardness (by precipitation hardening [11, 20]. Due to aging grain size increases, which provides more dislocation bowing, effectively increases its hardness [11].

4.1.3 XRD Analysis

Fig. 9 represents the diffraction peaks of AR, AA-FSP and AA-FSPZrO_2 composite, which are obtained using the XRD analyser. The diffraction patterns of as received specimen exhibit four major peaks at an angle (2θ) of 39°, 45°, 65° and 78°, with the corresponding to planes of (1 1 1), (2 0 0), (2 2 0) and (3 1 1) for aluminium [25]. It confirms the FCC crystal structure of aluminium. Due to the presence of a small amount of Si, Mg and Fe, there are some minor peaks of Mg_2Si, FeSi and Si.

After FSP, there is an increase in intensity at an angle (2θ) of 39° while intensity at other peaks is decreased. It may be due to dynamic recrystallization [25]. Zr has the lowest diffusion coefficient in aluminium due to which it forms very a small amount of Al_3Zr. The peak at 40.3° confirms the formation of Al_3Zr [22, 23]. This Al_3Zr present in the form of tetragonal structure in the aluminium matrix.

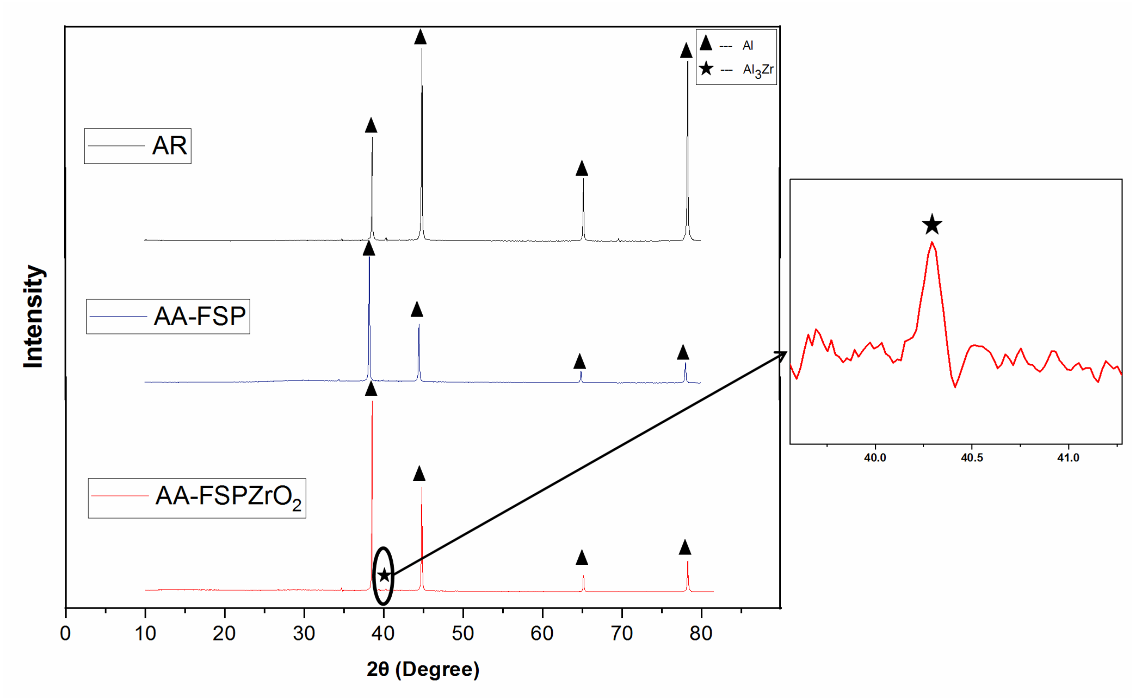

Fig. 9 X-Ray Diffraction patterns of as received and FSPed Al 6060 alloy.

4.1.4. Wear Analysis

Specimens AA, AA-FSP and AA-FSPZrO_2 were subjected to reciprocating wear under loading conditions of 10N and 15N. Dry wear was carried out for 20min. time, 3Hz frequency keeping radius 20mm for every specimen. AA-FSPZrO_2 shows least wear rate due to presence of hard surface which provides resistance to deformation. AA-FSP shows more wear than AA specimen. It is due to increase in roughness after FSP. There is a small increment in hardness of AA-FSP specimen, which can't oppose wear loss occurred due to high roughness. Increasing load causes more wear loss. At higher loading, specimens show higher wear loss than lower loading condition. Higher loading causes quicker removal of FSPed region which causes increase in contact area. Effectively it increases wear loss as well as COF. According to Prabhu et al [9], worn debris helps to reduce contact area between specimen and ball which affects decrease in COF.

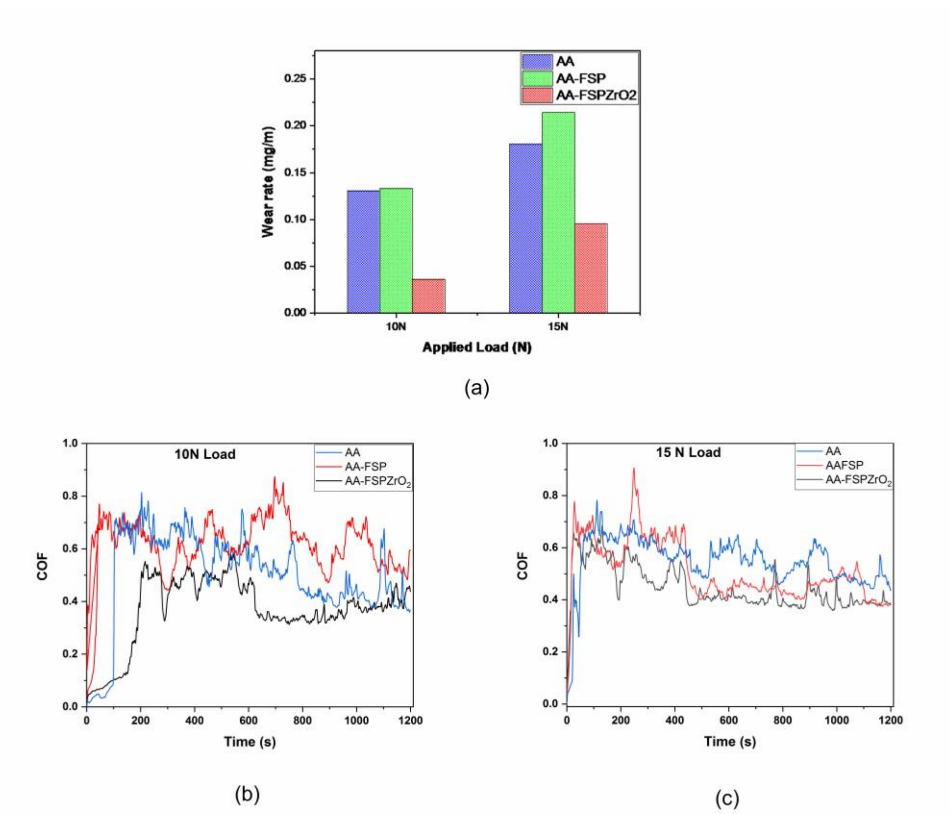

Fig. 10 Wear rate and COF of FSPed specimens.

4.2 Texturing, SMAT and Anodizing

4.2.1 Macrostructure

Surface texturing is obtained by two different processes - By using 1) WEDM, 2) SMAT. Macrographs of textured patterns formed by using WEDM and SMAT are shown in Fig. 3. Depths of grooves formed by WEDM texture and surface roughness by SMAT were measured by using 2D surface profilometer (Make: Taylor and Hobson, 315). Specimens textured by using WEDM measured the localized average depth of 50µm, 100µm and 150µm respectively at the position of grooves. While in the case of SMATed specimen, indentations (by the impact of moving balls) has shown the maximum depth of 10µm with an average surface roughness of 1.25 µm. After anodizing, there was a formation of porous Al_2O_3 which provides extra roughness to the specimens. 2D profiles of all these specimens are shown in Fig. 11.

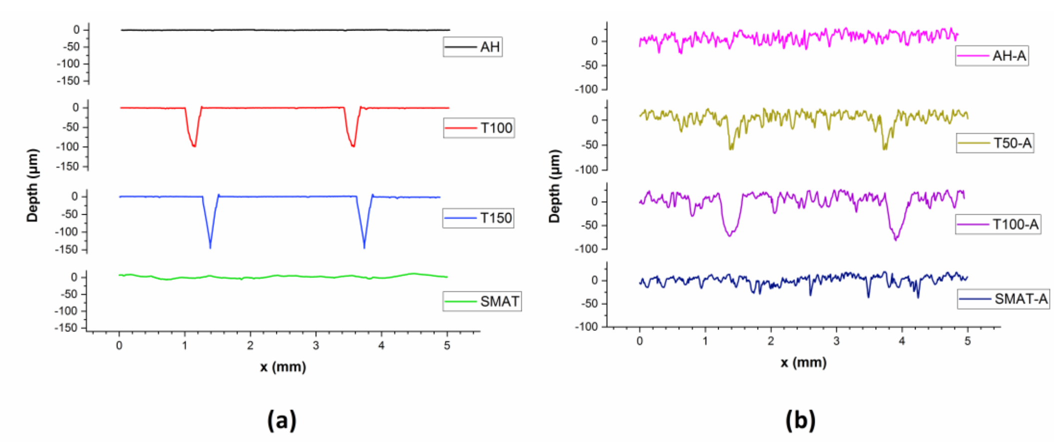

Fig.11 2D profiles of (a) non-anodized (b) anodized specimens.

4.2.2 Hardness

For homogenization as received specimens were solution heat-treated (heated at 530°C for 2 hours followed by water quenching). Hardness after solutionizing found to be 54.7HB. Variation in hardness values after texturing is shown in Fig. 12. There is a considerable increment in hardness when SMATed and a small change in hardness when textured by using WEDM. Since the surface was subjected to severe impacts during SMAT, it provides grain refinement in SMATed region. Effectively it increases the hardness of aluminium surface [1]. After 30 min of SMAT, hardness of as heat treated aluminium increased up to 66 HB. After anodizing of porous Al_2O_3 over aluminium surface, there is no considerable change in hardness.

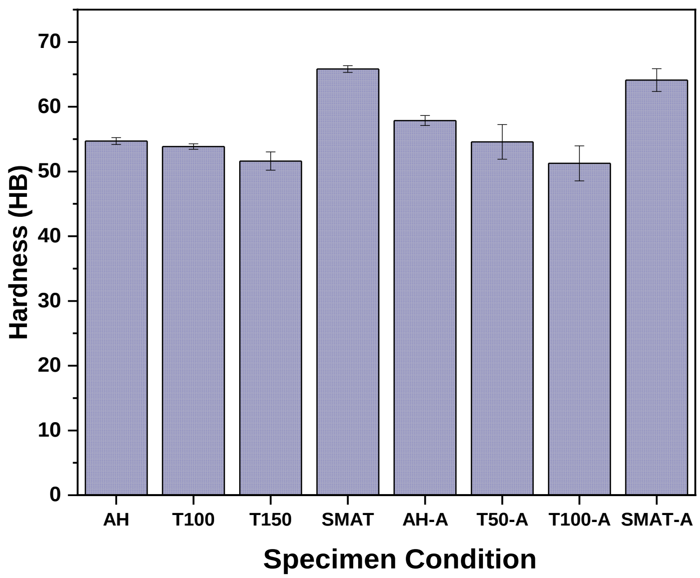

Fig. 12 Comparison of surface hardness of textured and non-textured specimens.

4.2.3 XRD Analysis

Fig. 13 represents the diffraction peaks of as received and anodized aluminium specimens, which are obtained using the XRD analyser. The diffraction patterns of as received specimen exhibit four major peaks at an angle (2θ) of 38.7°, 44.9°, 65.2° and 78.23°, with the corresponding to planes of (1 1 1), (2 0 0), (2 2 0) and (3 1 1) for aluminium [25]. It confirms the FCC crystal structure of aluminium. Anodized specimen showed all aluminium peaks similar to as received specimen with some small peaks of γ-Al_2O_3 at 40.1°, 58° and 69.4° [26]. γ-Al_2O_3 has FCC crystal structure.

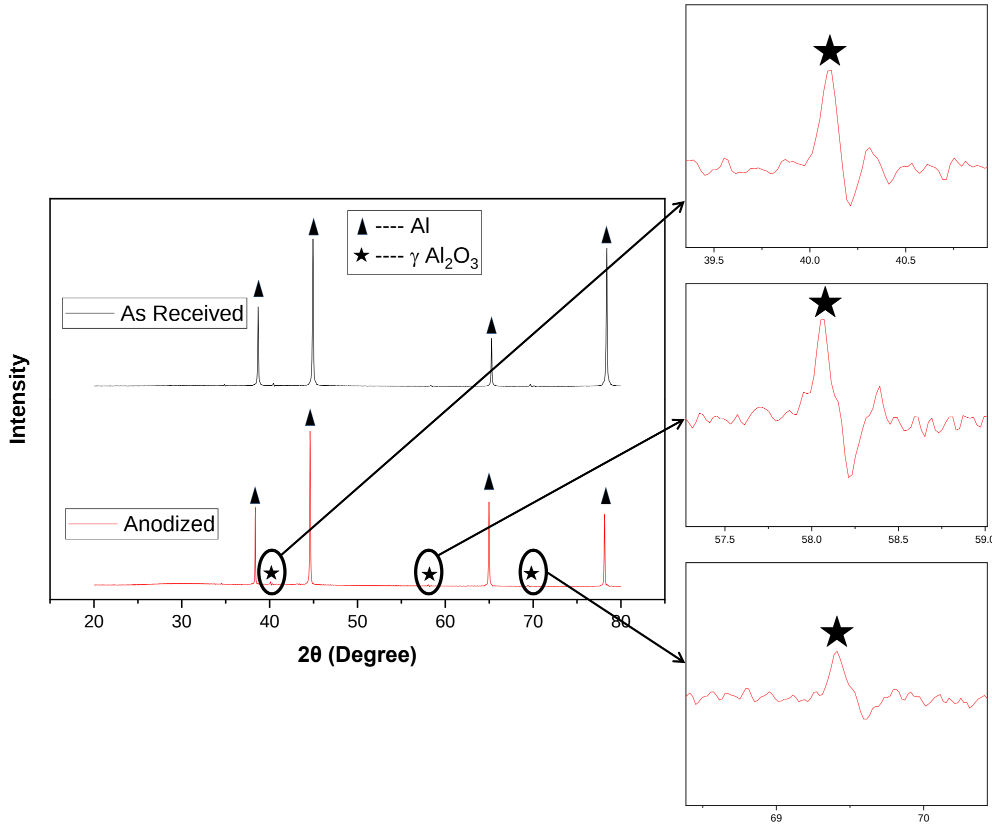

Fig. 13 X-Ray Diffraction patterns of As Received and Anodized Al 6060 alloy.

4.2.4 Wear and Frictional Analysis

Quantitative analysis of wear rates was carried out by using volume loss method. Initially area loss was measured with the help of 2D profilometer. 2D profiles of wear tracks are shown in Fig. 14 (curvy shape shows material loss by wear). Volume loss is calculated by using formula,

$$\text{Volume Loss} = \text{Area loss} \times 2\pi r$$

Where, r is radius of wear track (r = 10mm for lubricated wear condition while r = 20mm for dry wear condition).

SMAT-A specimen show shallower curves than other specimens which provide it lower area loss. Eventually it shows lower volume loss under both dry and lubricated conditions than others. Comparison of volume losses in both lubricated and dry conditions are shown in Fig. 15.

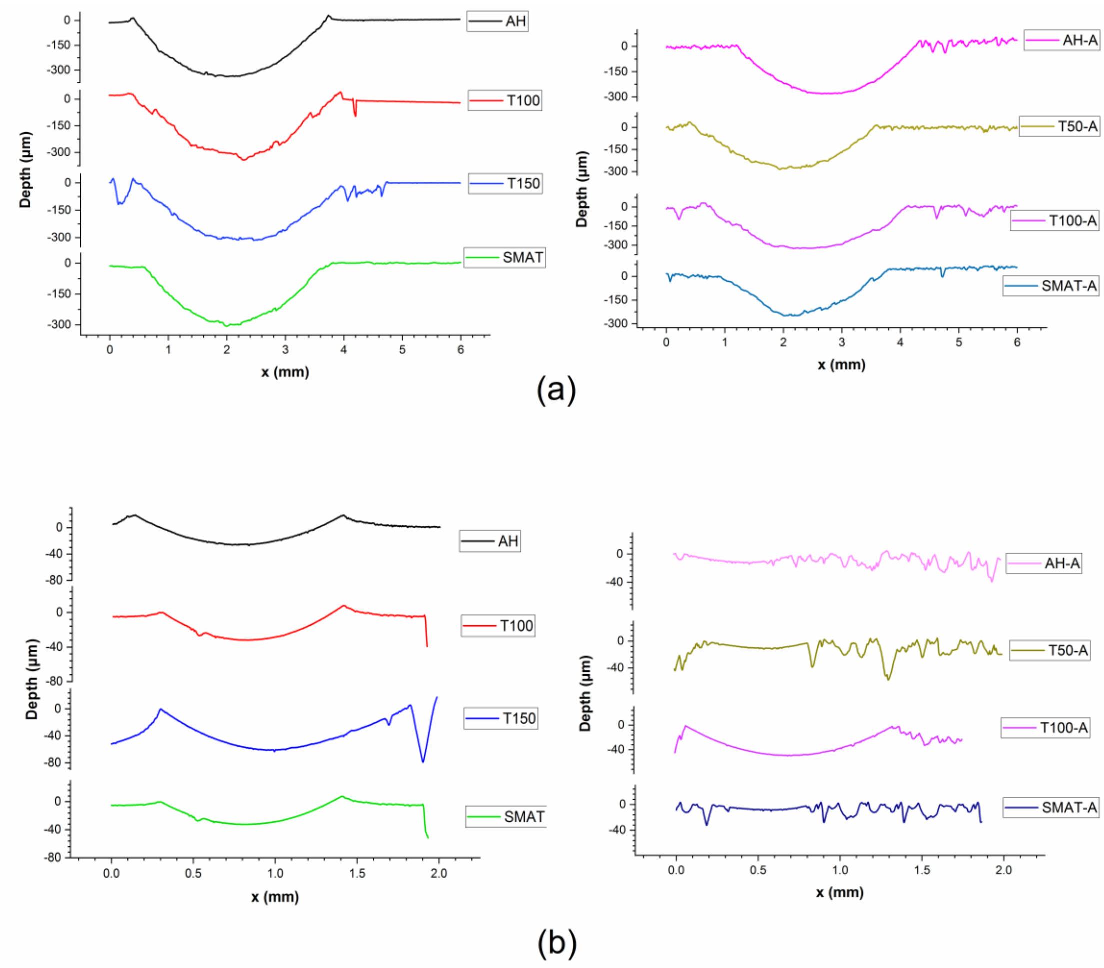

Fig. 14 2D profiles of area loss under (a) dry condition and (b) lubricated condition.

Specific wear rate under both dry and lubricated condition was calculated by using formula,

$$\text{Specific Wear Rate} = \frac{Volume\ Loss}{Applied\ Load \times Total\ distance\ covered}$$

Comparison of specific wear rate is shown in Fig. 15.

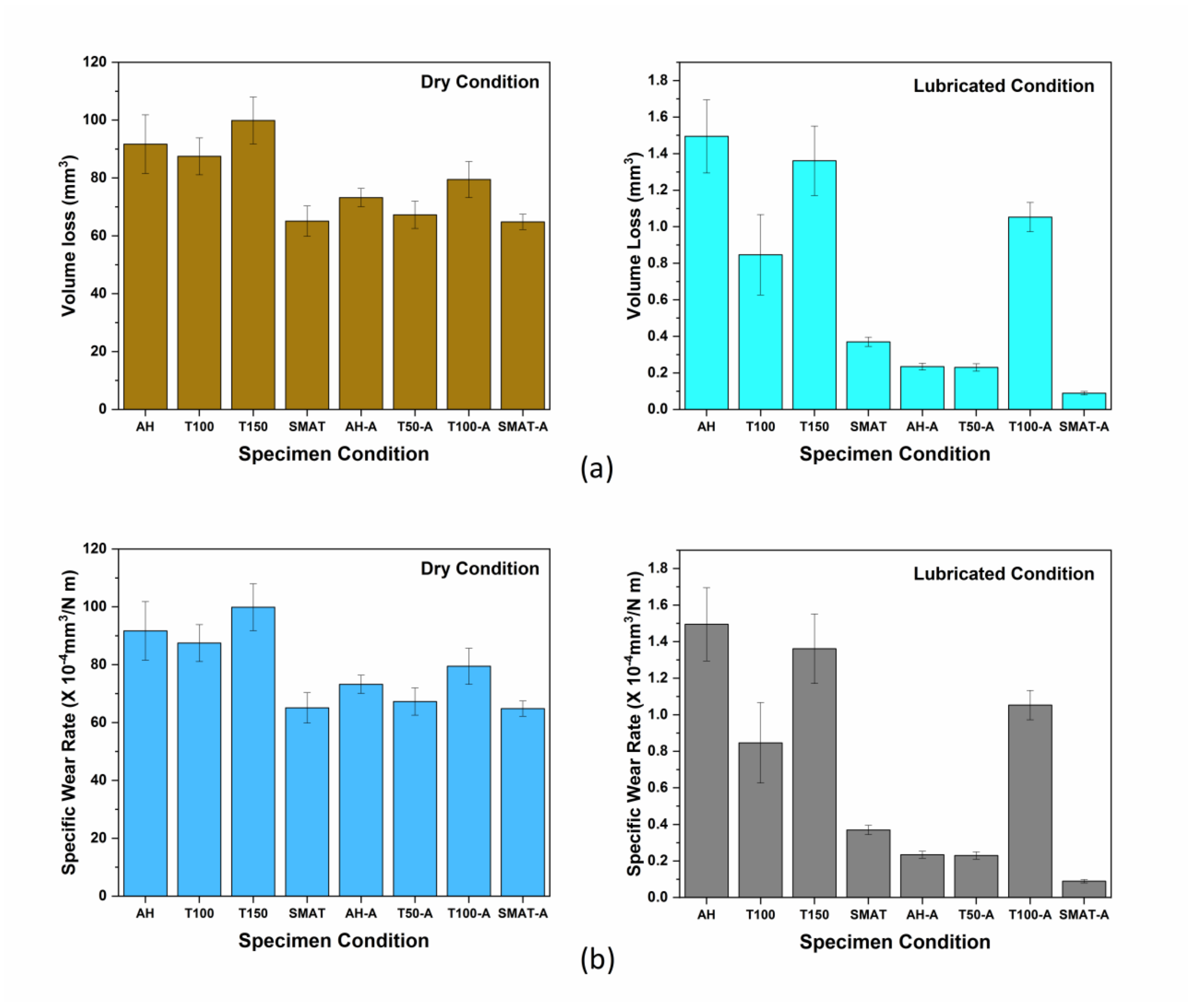

Fig. 15 (a) Volume Loss and (b) Specific wear rate for both dry and lubricated condition

As shown in Fig. 15, under dry condition, AH specimen have specific wear rate of 91.7 × 10^{-4} mm^3/N.m. Wear of every specimen starts with Flattening. Flattening is the phenomenon of increment in contact area between ball and specimen surface which occurs as shown in Fig. 16. Contact area between ball and metal surface is less at the starting of wear which increases due to applied pressure as process goes further. However, for textured specimens, there is an increase in localized pressure when ball comes in the contact of edges of textured grooves. Due to wearing of edges in the initial stages, textured specimens shows more wear rate than that of other specimens. U. Pettersson et al. [27] has shown, when ball and surface come into contact, the amount of deformation and wear depends on the properties of the materials (hardness and elasticity of the sliding pair and the difference in hardness between the two materials). Due to high hardness, specimen surface resist deformation results in lower wear loss. SMATed specimen showed increment in hardness after processing which provided lesser wear loss.

After anodizing wear rate of the AH-A specimen decreased up to 73.23 × 10^{-4} mm^3/N.m, which is an increment in wear resistance by 20%. Wear rate for anodized specimens is lower than that of non-anodized specimens. It is due to formation of hard and wear resistive Al_2O_3 layer above aluminium surface. Al_2O_3 layer on the aluminium surface avoid direct contact of ball and aluminium surface in the initial stages of wear. Strong anodized layer provides more wear resistance to the anodized specimens than non-anodized specimens [28]. In case of SMAT-A specimen, combination of SMAT and anodizing provide it best wear resistance up to 64.81 × 10^{-4} mm^3/N.m which is 30% better than AH specimen.

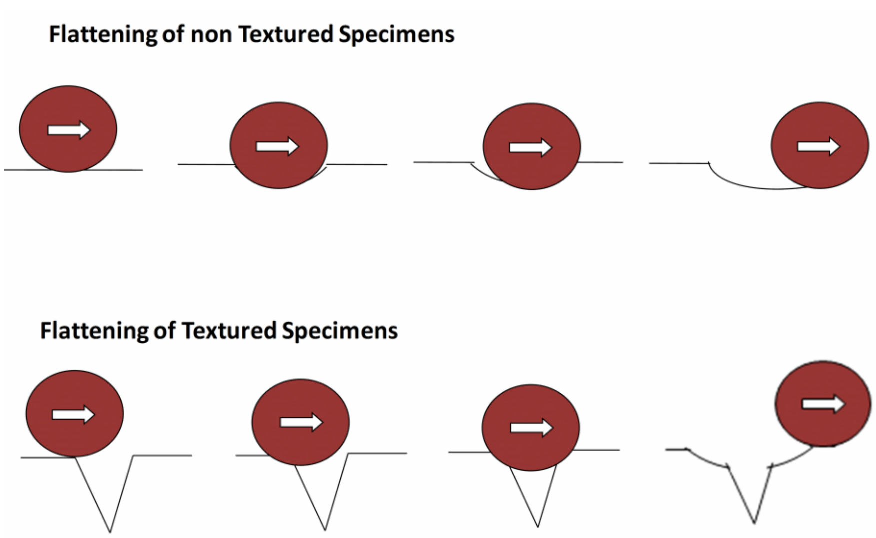

Fig. 16 Flattening steps during wear.

Friction between ball (pin) and specimen surface plays important role in wear behaviour. Generally, wear is a result of ploughing, adhesion and abrasion.

Coefficient of friction (COF) is one of the important factors in tribological studies. COF is frictional force between ball and specimen surface per unit applied normal force by ball on surface. It was measured by wear apparatus itself. Fig. 17 shows variation of COF with respect to time of loading. Reduction in COF by increasing loading time is due to softening of material because of localized thermal heat produced during friction [29]. Thus the COF drop down gradually with respect to time.

Under dry condition, COF show fluctuations which may be due to formation and removal of material particles onto the ball (pin) [29]. Both anodized and non-anodized specimens show an increment in COF in initial stages and then reach steady state after some time. It may be due to direct contact of ball and specimen surface during flattening phenomenon. However, T100-A specimen show increase in COF because wear mechanism is adhesive followed by abrasive in later stages [29].

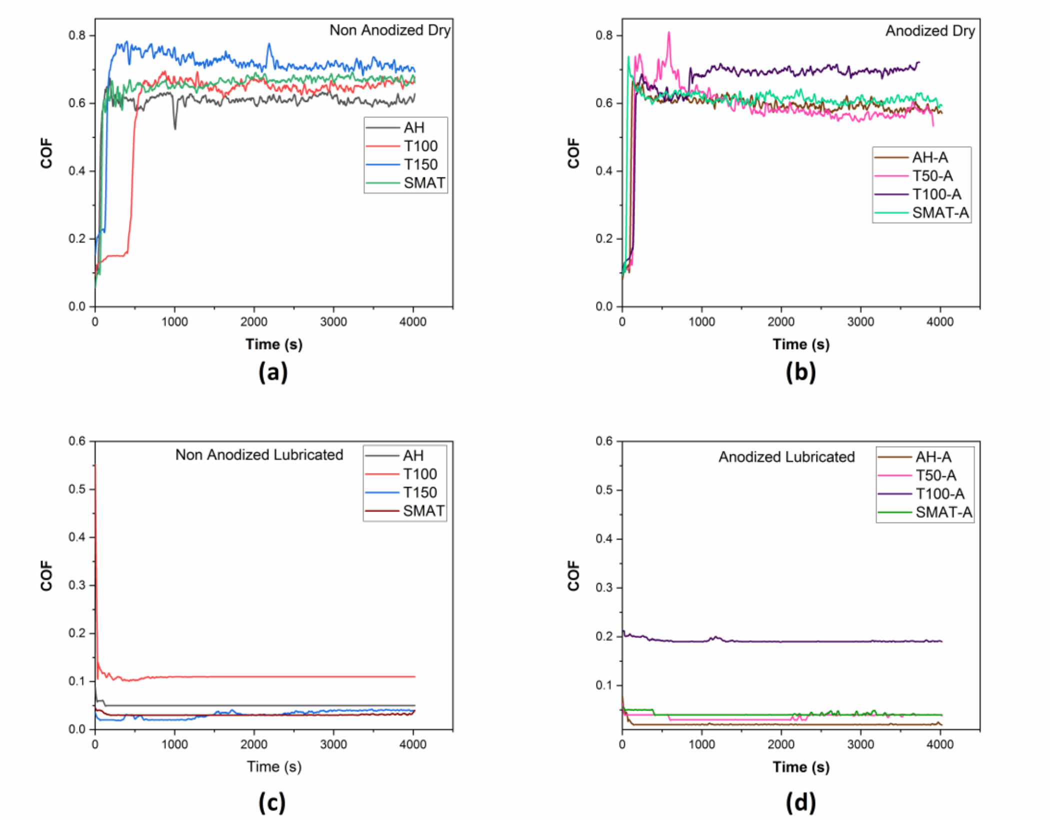

Fig.17 COF under dry and lubricated conditions

4.2.4.1 Wear Mechanism under Dry condition

Wear mechanism basically depends upon applied load, velocity and mechanical properties of specimen [30]. Wear mechanism can be identified with the help of SEM images of wear track. Fig. 18 shows SEM images of worn surface of AH specimen. Formation of shallow grooves, micro-cutting, adhesion of metal surface and formation of debris provides evidence that wear loss is due to combination of different wear mechanisms namely abrasive wear and adhesive wear. Fig. 18 (a) and (b) confirms mild adhesive and abrasive wear [31]. Fig 18 (b) and (d) shows the scuffing marks which occur due to frictional heat and adhesive wear. There is a temperature rise due to frictional force which causes localized softening of aluminium surface. Softening of aluminium surface occurs due to its lower surface hardness. Fig. 18 (b) shows formation of flaky debris.

Flaky debris is evidence of softening during wear. Softening of surface may causes removal of debris more severely than its formation [25]. Effectively this increases its wear loss. For higher loading distances, temperature rise causes agglomeration of particles [29]. Due to more softening during wear, COF of AH specimen is lower than the others [31].

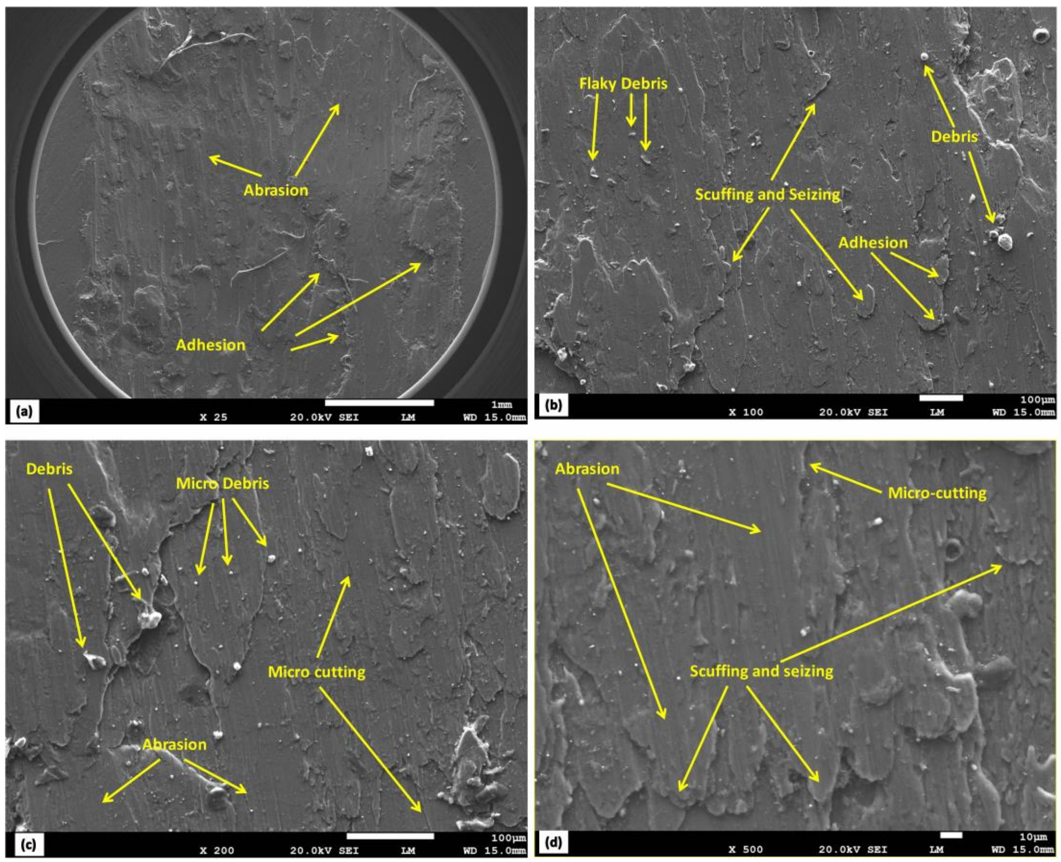

Fig. 18 SEM images of AH specimen wear track.

Fig. 19 shows SEM images of T100 specimen wear track. Severe abrasive groove formation in Fig. 19 (a) and mild adhesion confirms that the wear loss is due to combined effect of abrasive and adhesive wear. Wrinkle like abrasive marks are evidence of abrasive wear while prows like adhesive marks in Fig. 19 (b) and scuffing marks in (c) are evidence of adhesive wear mechanism. (c)

Shows micro-cracks and micro pits which may be due to either severe abrasion or due to mild erosive wear. Erosion is the striking of particle to the surface and rebounding from it, while abrasion is sliding of abrasive particles along surface under action of applied force [32]. Lesser prows like marks in T100 show lower softening in case of T100 than AH specimen. Effectively, wear loss by T100 is lesser than that of AH Specimen.

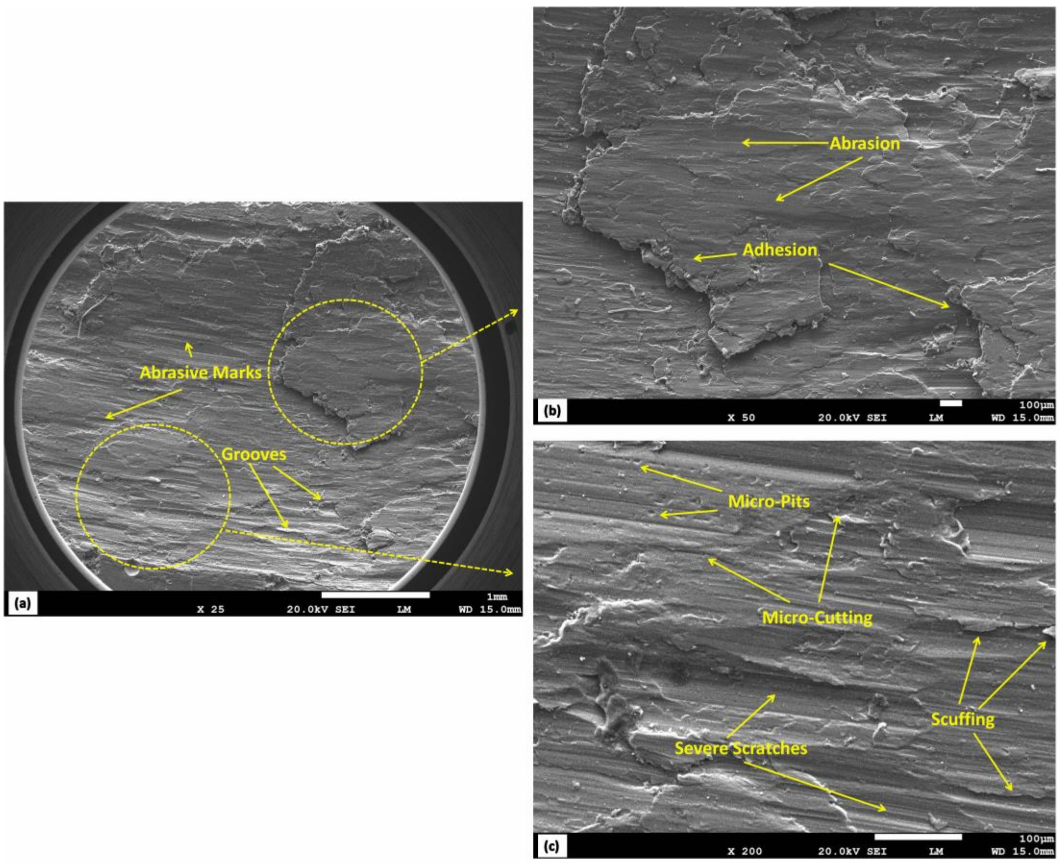

Fig. 19 SEM images of T100 specimen wear track.

SEM images of worn surface of T150 specimen in Fig. 20 show wear mechanism is mainly abrasive. Wear is mainly due to abrasion followed by mild adhesion. Due to more abrasive wear than AH and T100 specimen, total wear loss by T150 is more. Formation of micro-particles, debris, shallow grooves shows abrasive and adhesive wear. Shallower grooves along sliding direction and matrix debonding are due to abrasive wear. Scuffing and seizing marks or micro-cutting marks shows dominance of abrasive wear. Size of debris is smaller than the debris in AH specimen. It is due to initial cutting of brittle textured edges. Due to less softening and failure, debris is smaller and in larger quantity.

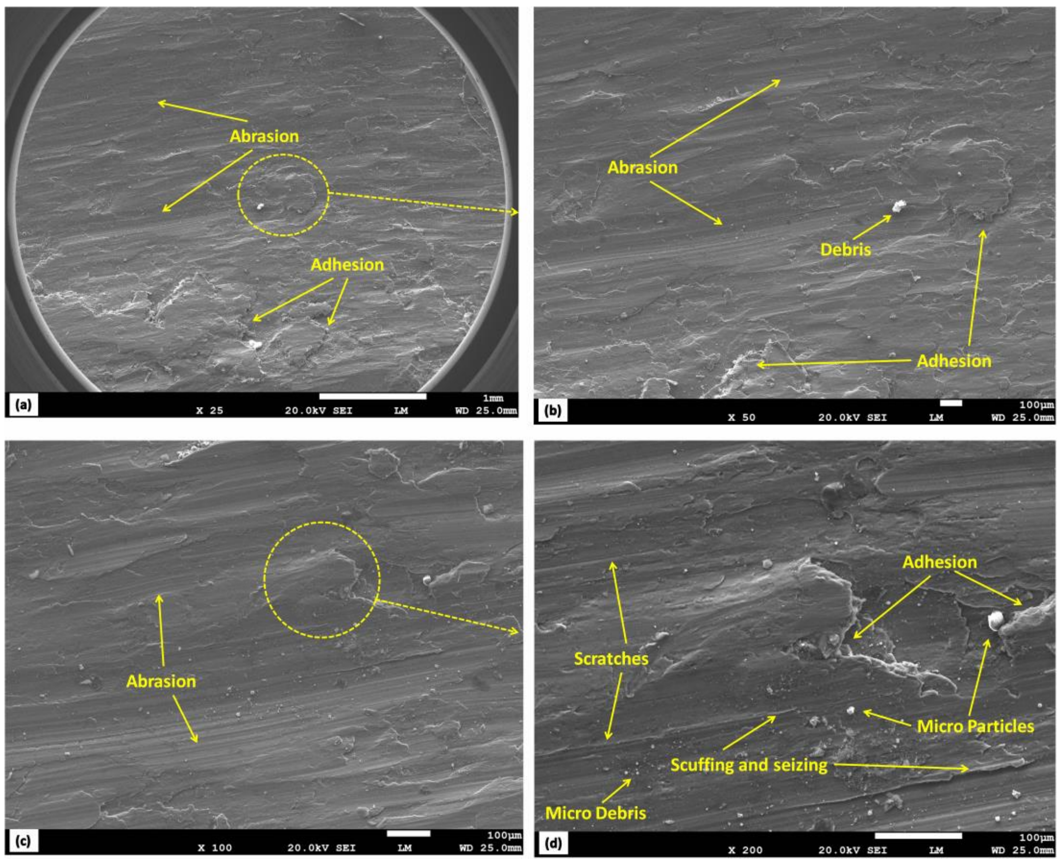

Fig. 20 SEM images of T150 specimen wear track.

Worn SMATed specimen in Fig. 21 (a) shows deeper grooves and severe abrasive marks while that of Fig. 21 (b) and (c) represents severe adhesive marks. So, in case of SMATed specimen wear is due to both combination of abrasion and adhesion. Severe adhesive marks and brittle fracture shown in Fig. 21 may be due to higher hardness of SMATed specimen than others. Fragmentation and debris formation is mainly due to adhesive wear. More hardness of specimen is beneficial in increasing load bearing capacity which can effectively reduce wear loss [29]. Due to this SMATed specimen shows 29% more wear resistance than AH specimen.

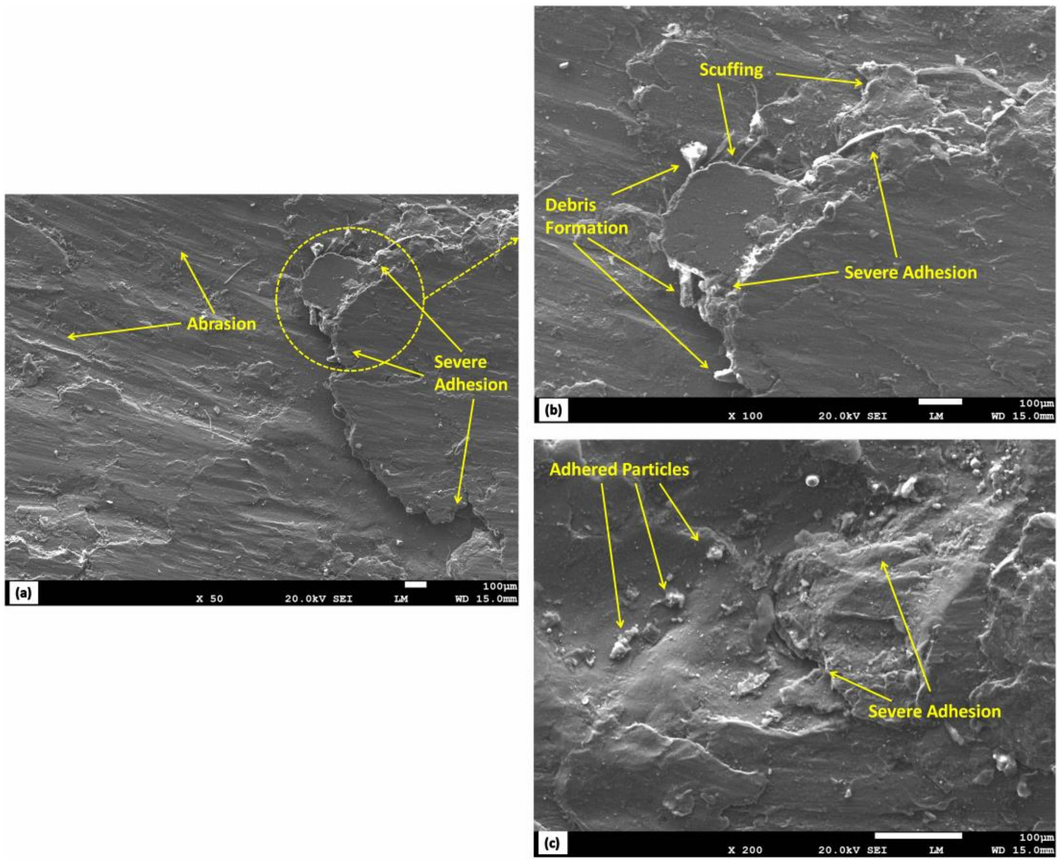

Fig. 21 SEM images of SMATed specimen wear track.

For AH-A specimen, SEM images in Fig. 22 shows shallower abrasive marks with large number of adhered particles. Presence of many adhesive marks evident about adhesion to be dominant wears mechanism. Severe adhesive marks are due to hard brittle surfaces. Formation of spherical adhered particles may shows presence of oxidative wear [29]. SEM images show more quantity of debris in case of AH-A specimen than AH specimen. Debris in anodized specimen is harder and brittle, which doesn't show softening. Instead it breaks into smaller and smaller debris. Fig. 22 (d) shows presence of many micro-pits at a particular region within worn surface. It may be due to severe abrasive or mild erosive wear [28]. Micro-cracks and scuffing is due to abrasion over hard and brittle anodized layer. Eventually, due to presence of hard anodized coating, wear loss by AH-A is lesser than AH specimen.

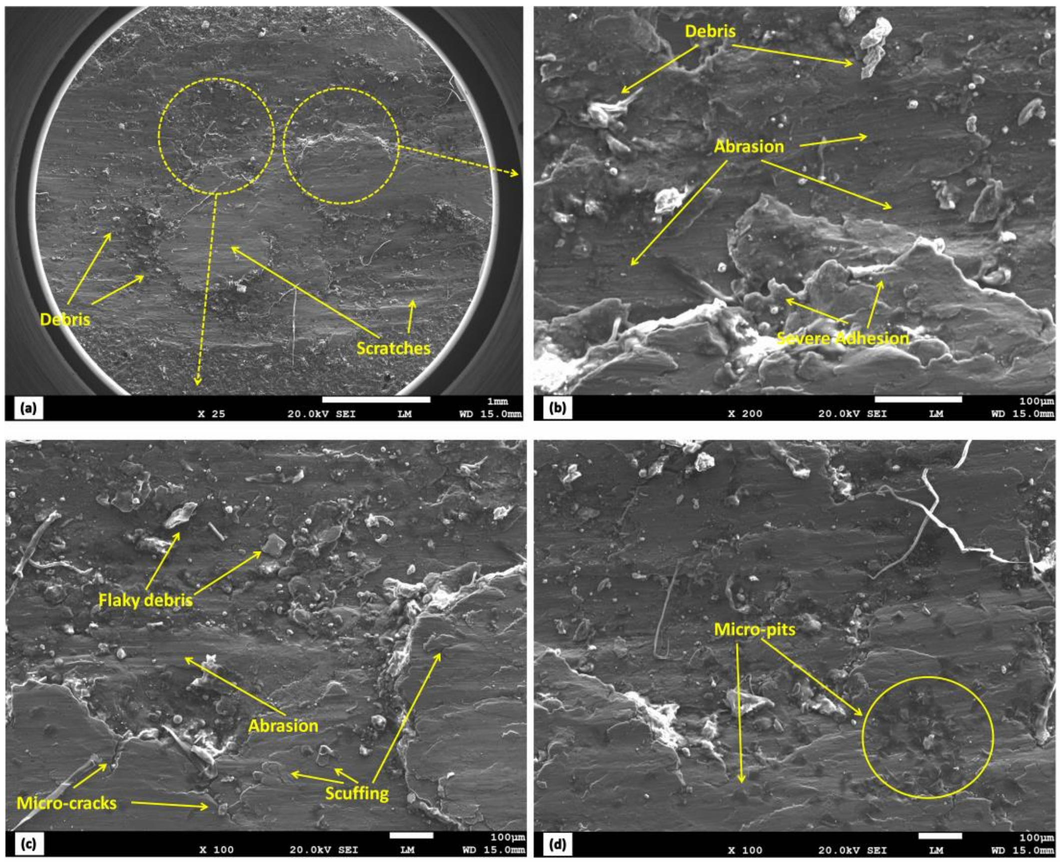

Fig. 22 SEM images of AH-A specimen wear track.

SEM images in Fig. 23 shows worn out surfaces of T50-A specimen. Presence of majority of scratches, micro-cracks shows dominant wear mechanism to be abrasive. Prows like marks and adhesive marks in Fig. 23 (b) shows presence of adhesive wear. Shallower scratches, lower adhesion provides lower wear loss of T50-A specimen than AH-A specimen. Micro-cuttings and smaller debris are due to abrasive wear hard anodized surface. Small quantity of hard debris than other anodized specimens provides lower frictional force which effectively reduces its COF.

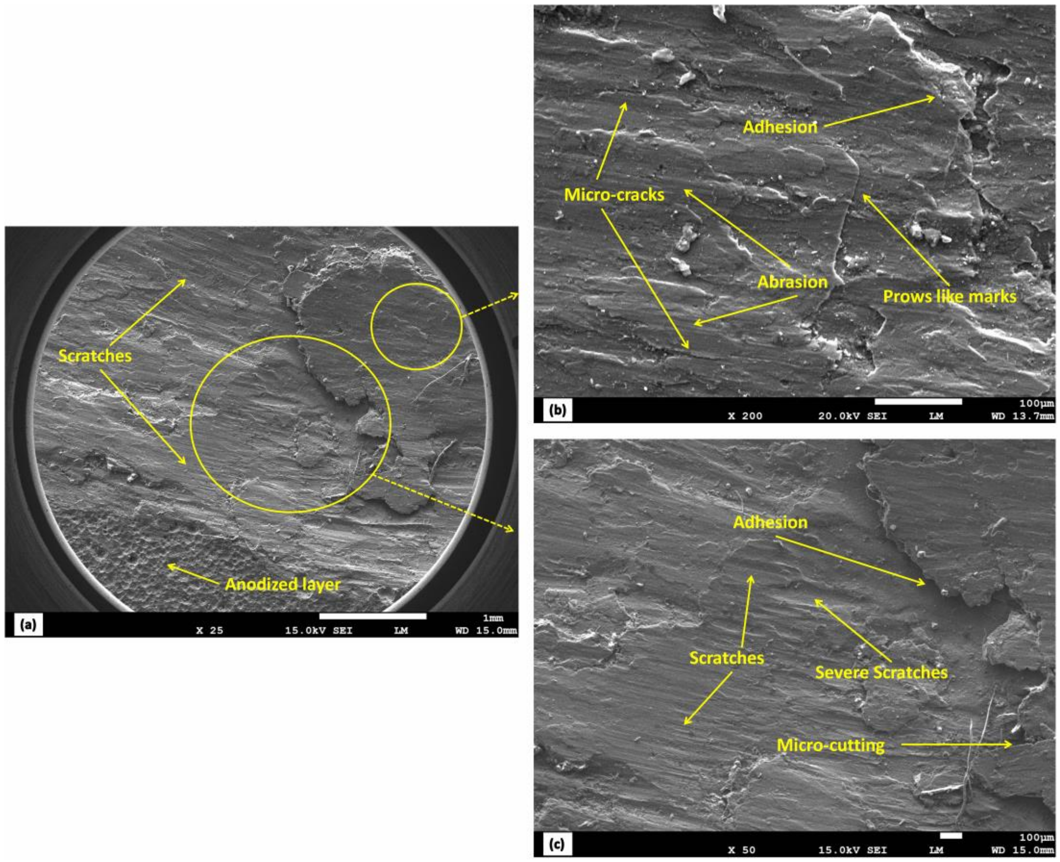

Fig. 23 SEM images of T50-A specimen wear track.

Fig. 24 shows SEM images of wear track of T100-A specimen. Three different wear mechanisms namely abrasive, adhesive and mild erosive wear observed to coexist on the basis of abrasive and adhesive marks, micro-cuttings, cracks and formation of micro-pits. Formation of cracks and micro-cuttings are due to brittle anodic layer while micro pits are effect of penetration of hard particles due to applied force. Formation of severe scratches and cracks shows abrasive wear to be dominant. Because of higher abrasive wear, wear loss in

T100-A specimen is more than that of AH-A specimen. Moreover, presence of harder debris increases COF of T100-A specimen.

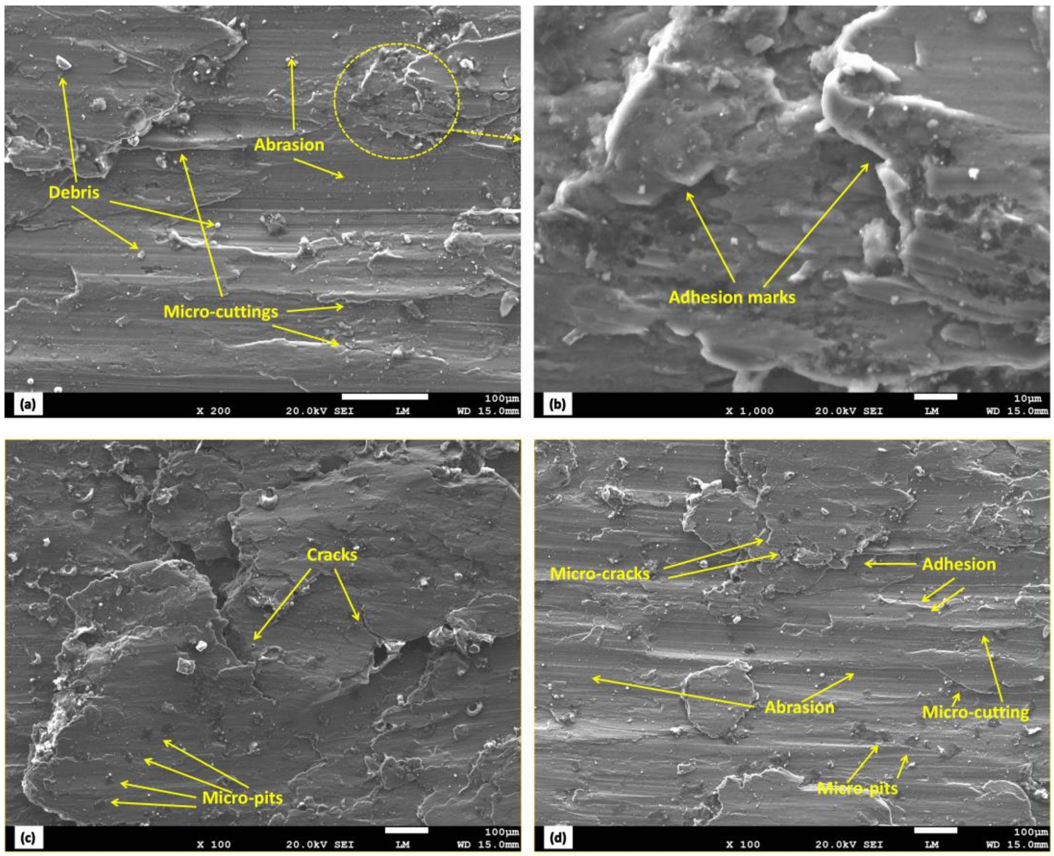

Fig. 24 SEM images of T100-A specimen wear track.

SEM images of SMAT-A specimen shown in Fig. 25 shows wear mechanism to be mainly abrasive with presence of mild adhesive wear. Shallower scratches are due to abrasion of debris over very hard surface. Scuffing and seizing occurs due to mild adhesion followed by abrasion. Formation of debris shown in Fig. 25 (c) is due to combined abrasion and adhesion of brittle hard layer formed by SMAT and anodizing. SEM clearly shows lower abrasive and adhesive marks in SMAT-A specimen than others, also area loss shown in (a) is lesser than others, which provide it lowest wear loss.

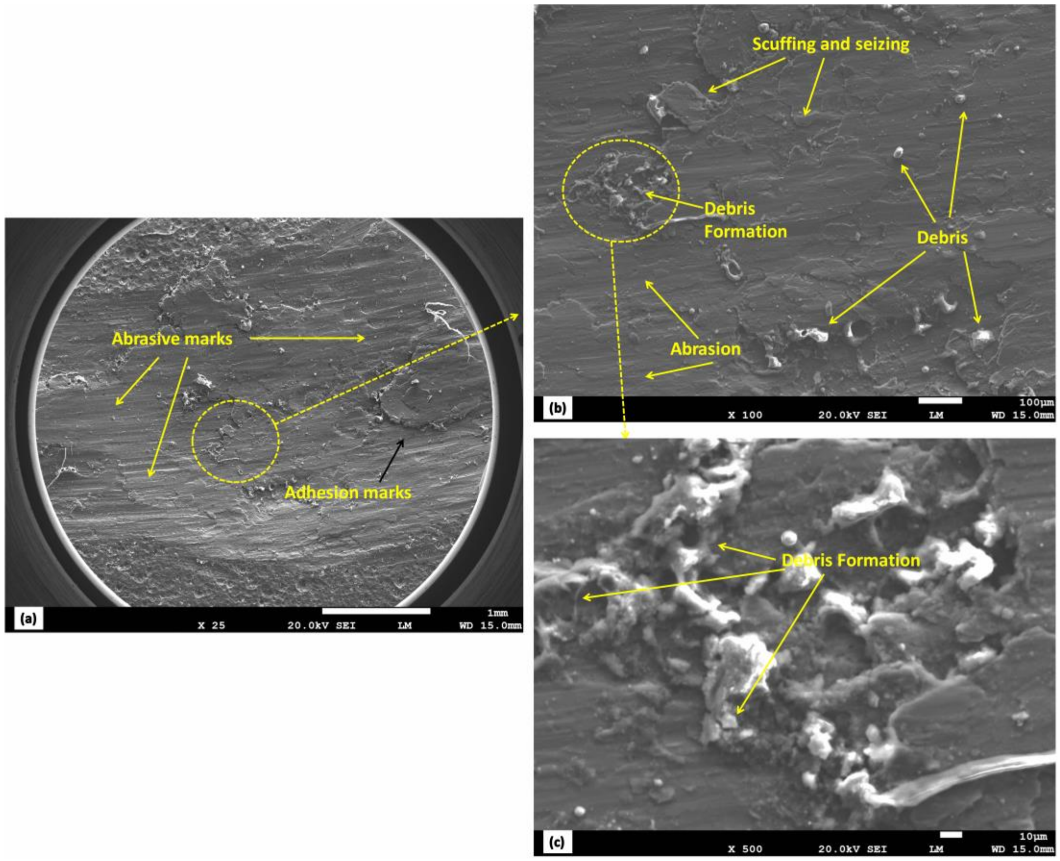

Fig. 25 SEM images of SMAT-A specimen wear track.

4.2.4.2 Wear Mechanism under Lubricated condition

Lubricated wear tests were carried to study the influence of lubricant on tribological properties of textured, SMATed and anodized specimens. Lubricated wear mechanisms can be explained by 3 types of lubrication systems namely (1) Boundary Lubrication, (2) Mixed Lubrication, (3) Hydrodynamic Lubrication. These systems can be differentiated with the help of Stribeck curve (Fig. 26, [33]). Initially, every tribological system starts with boundary lubrication followed by mixed lubrication and hydrodynamic lubrication [34]. H. L. Costa et al. [35] has shown that initially COF increases and after some sliding distance it decreases during boundary lubrication. Further reduction in contact area shifts mixed lubrication to hydrodynamic lubrication. Wear mechanism for boundary lubrication is combination of adhesion and abrasion while during hydrodynamic lubrication, it shows abrasive wear mechanism [36].

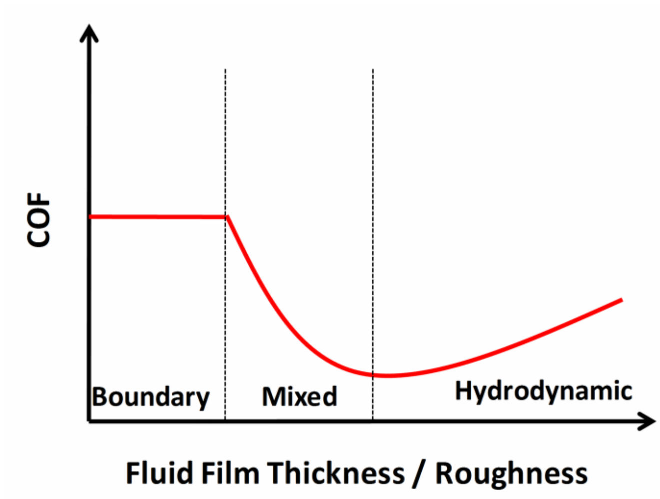

Fig. 26 COF variation according to different lubrication conditions.

AH specimen shows specific wear rate of 1.49×10^{-4} $mm^3/N.m$. Textured and SMATed specimens show lower wear loss in case of non-anodized specimens (Fig. 15). It is due to accumulation of lubricant within grooves which provide it lower contact area between ball and specimen. Eventually it reduces their wear loss. In case of SMATed specimen, lower wear loss is due to its increased hardness after SMAT. SMAT specimen show specific wear rate of 0.37×10^{-4} $mm^3/N.m$ which is four times lower than AH specimen. Anodizing provides more wear resistance to anodized specimens due to formation for hard Al_2O_3 coating over aluminium surface. AH-A specimen shows specific wear rate of 0.23×10^{-4} $mm^3/N.m$. Further reduction in wear loss is obtained by combination of SMAT and anodizing. It shows specific wear rate of 0.09×10^{-4} $mm^3/N.m$ which is 16 times lower than AH specimen.

As shown in Fig.27 wear mechanism starts with the wear of texture edges. During this condition, there is an increase in pressure at the inlet and exit of grooves. It is due to lower accumulation of lubricant within grooves which provides more contact area between specimen and ball (pin). This type of contact is known as non-conformal contact. The higher wear rates (during boundary lubrication) observed for the textured surfaces resulted in a faster transition from non-conformal to conformal contact. It is beneficial because it promotes accumulation of lubricant within textured grooves (created by WEDM) or dimples (created by SMAT), which significantly reduces COF due to growth of lubrication film [37, 38].

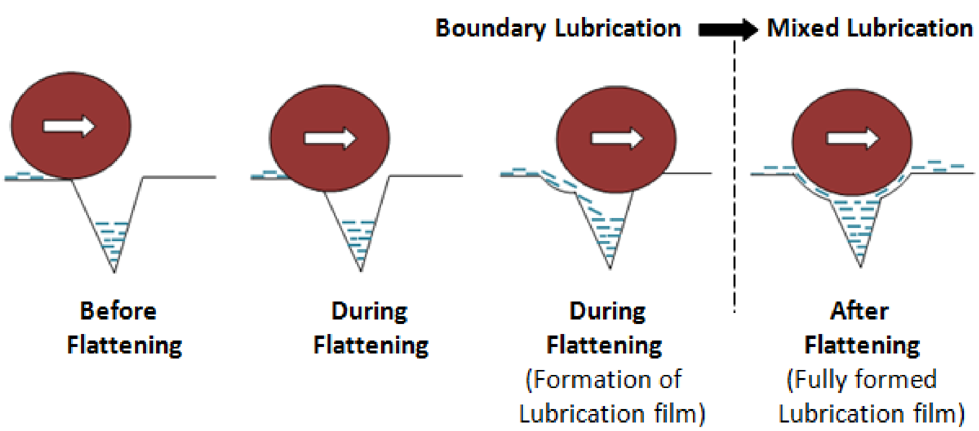

Fig. 27 Flattening mechanism for lubricated condition.

According to Ping Lu et al. [38], the low depth textures provide lower wear loss because of lower flattening as compared to deeper textures. When the ball (pin) crosses the groove/dimple, it retains some lubricant in the groove back. This retained lubricant provides a further reduction in COF. This effect is called as secondary lubrication. Due to this fact, circular and oval shaped textures provide better wear resistance and lower COF [38]. This is one of the reasons behind less COF in SMATed specimen than other non-anodized specimens.

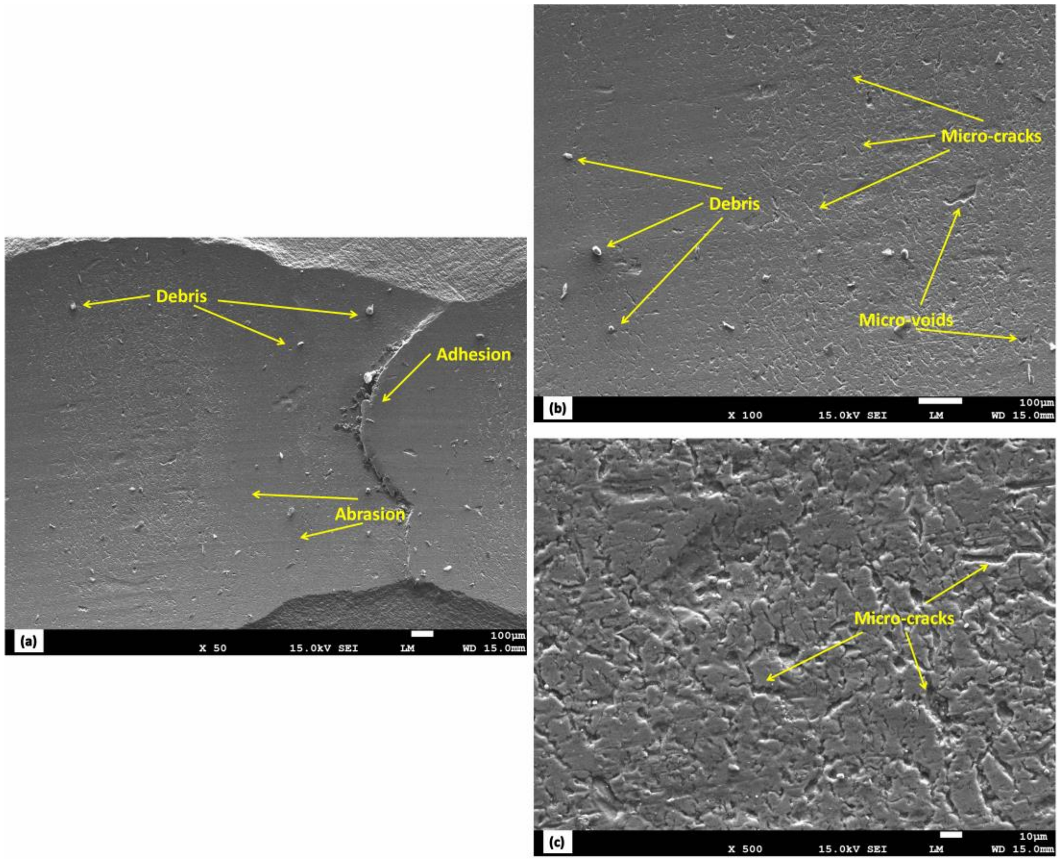

Fig. 28 SEM images of AH specimen - lubricated wear track.

Worn surface of AH specimen under lubricated wear is shown in Fig. 28. Mainly it shows presence of scratches, micro-cracks and debris. It is the evidence for dominance of abrasive wear. Fig. 28 (a) shows presence of adhesive marks which shows mild adhesive wear. Micro-cracks in (b) and (c) are due to abrasive wear. These cracks propagate and may connect to detach small wear debris [39]. This causes formation of micro-voids. According to Bermudez et al [40], under lubricated condition, bare aluminium shows combined adhesion and abrasion wear mechanism and it may follow oxidation of wear debris.

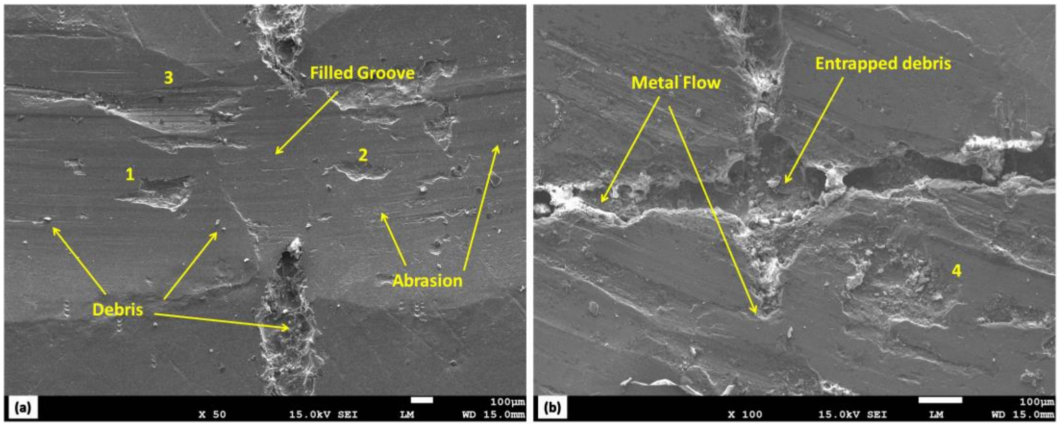

Fig. 29 SEM images of T100 specimen - lubricated wear track.

As shown in Fig. 29, abrasion is the dominating wear mechanism for T100 specimen under lubricated condition. Here, SEM shows that after lubricated wear for 1000 m, grooves of T100 specimen are getting filled due to metal flow which stops supply of secondary lubricant. Moreover contact area between ball and metal is also increasing due to metal flow. Grooves marked from 1 to 4 shows application of higher impact before entering and after exiting grooves, which increases its frictional force. Eventually, COF of T100 specimen is more than others.

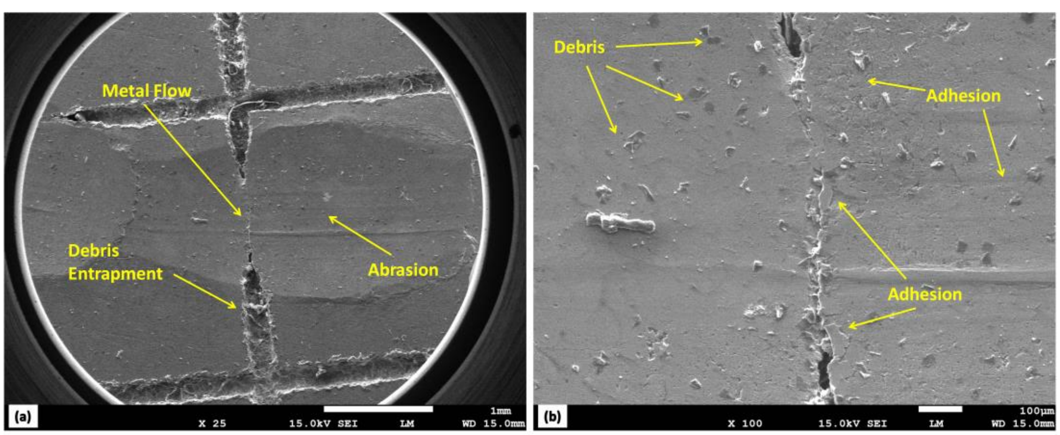

Fig. 30 SEM images of T150 specimen - lubricated wear track.

Fig. 30 shows SEM images of wear track of T150 specimen after lubricated wear test. It shows presence of large amount of wear debris as well as shallow abrasive scratches. This show wear is caused by adhesion in initial stage followed by abrasive wear. More wear loss of T150 is due to more adhesion during flattening phenomenon. Same like T100 specimen, T150 also shows groove filling due to metal flow, but amount of flow in T150 is seems to be lesser than T100 specimen. So, effectively contact area in T150 less than that in T100. Also deeper textured grooves provide secondary lubrication, which reduces COF of T150 specimen. Moreover, literature has shown that textured grooves may provide entrapment of third body abrasives (debris) which helps to further reduce COF [14, 15].

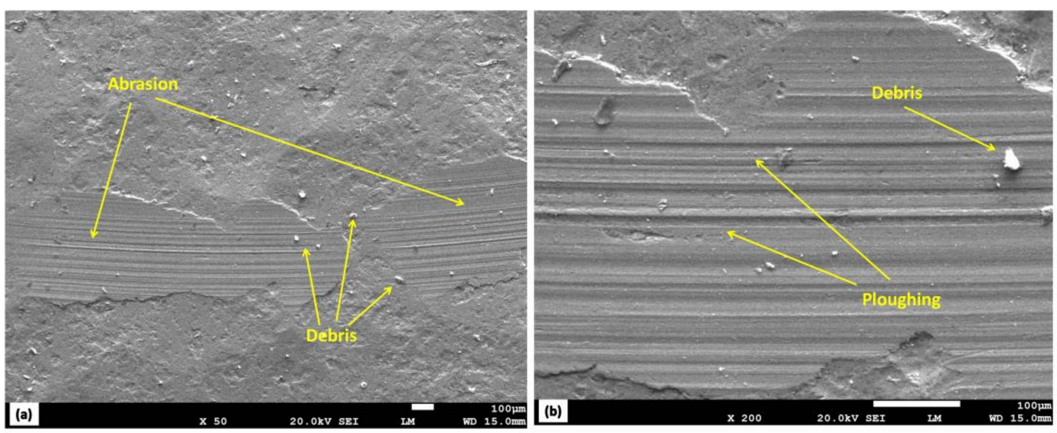

Fig. 31 SEM images of SMATed specimen - lubricated wear track.

SEM images of worn out surface of SMATed aluminium specimen shown in Fig. 31 clearly shows abrasive mechanism to be dominant wear mechanism. Fig. 31 (a) shows size of wear track in SMATed specimen is smaller than other non-textured specimens which provide it better wear resistance. It is due to more hardness of SMATed specimen [27]. More hardness opposes surface deformation. Lower contact area also provides it lower COF. (b) Show deep ploughing marks due to abrasion of hard debris. Size of debris in case of SMATed specimen is smaller as compare to others due to breaking of debris during wear instead of softening because of its higher hardness.

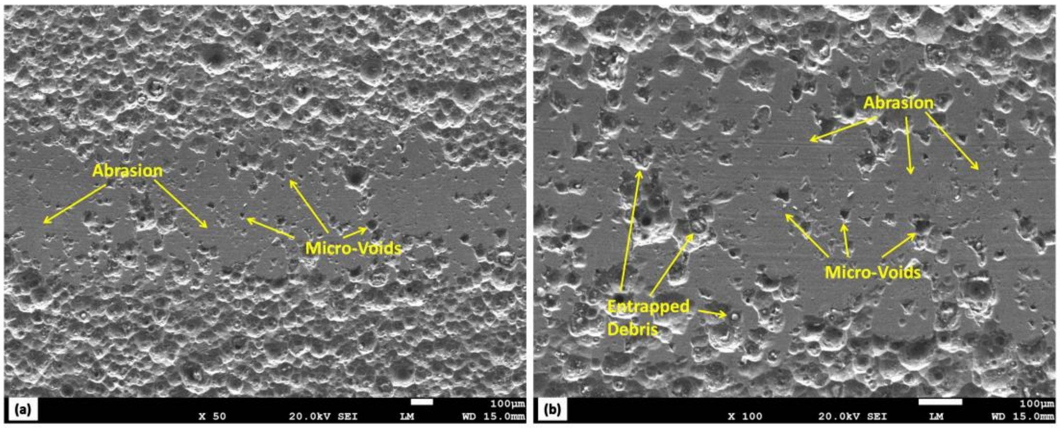

Fig. 32 SEM images of AH-A specimen - lubricated wear track.

Fig. 32 shows SEM images wear track of AH-A specimen after lubricated wear test. Presence of abrasive marks and micro-voids are evidence of abrasive wear. Absence of adhesion is may be due to presence of hard Al_2O_3 film over aluminium surface [19]. Size of wear track is less which provides it lower wear rate. AH-A specimen shows lowest COF among all specimens possibly because of following three reasons. First is lower contact area due to hard anodized surface. Second is presence of oval shaped micro-voids already formed due to anodizing provides it secondary lubrication [38]. And third may be entrapment of third body abrasives as shown in Fig. 32 (b).

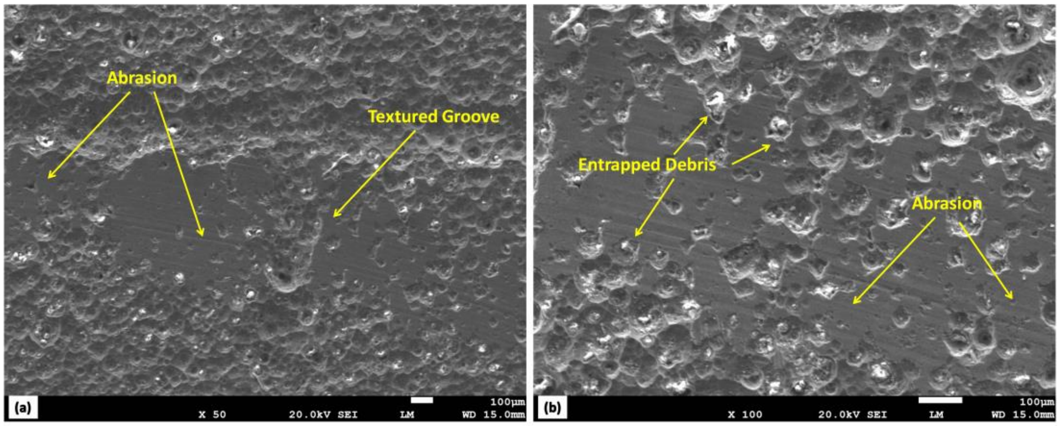

Fig. 33 SEM images of T50-A specimen - lubricated wear track.

Worn surface of T50-A specimen after lubricated wear test is shown in Fig. 33. It shows presence of ploughing like abrasive marks which confirms wear mechanism to be abrasive. Wearing of T50-A specimen is similar to that of AH-A specimen. T50-A also shows presence of oval shaped micro-voids and entrapment of wear debris which helps it to reduce its COF. T50-A doesn't show groove filling like non anodized textured specimens (T100 and T150). It may be due to absence of metal flow due to hard and brittle anodized Al_2O_3 coating. Moreover, anodized coating avoid direct ball to aluminium contact which provides better wear resistance.

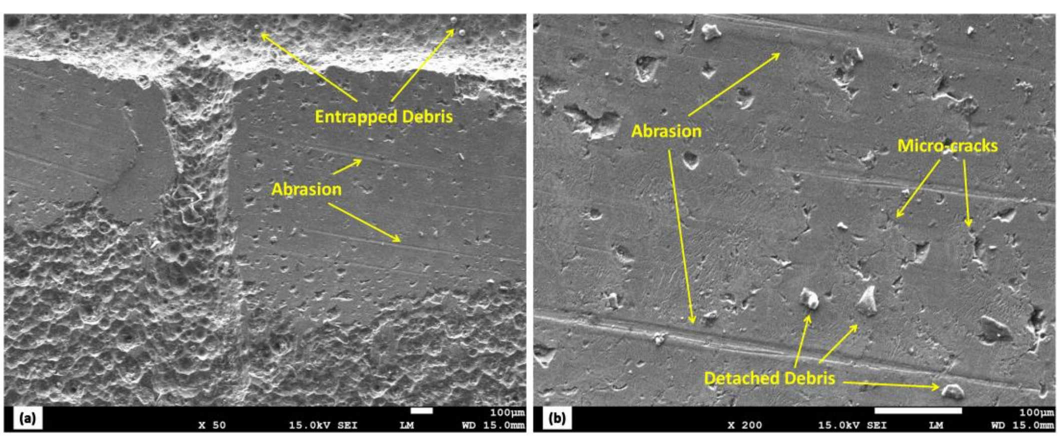

Fig. 34 SEM images of T100-A specimen - lubricated wear track.

As shown in Fig. 34, T100-A specimen shows abrasive wear mechanism. Wearing of surface is mainly due to detachment and abrasion of hard debris over surface. There is a formation of micro-cracks which propagate, connects each other followed by detachment of debris [39]. Due to deeper textured grooves, flattening of T100-A occurs more than that of other specimens due to which T100-A shows higher volume loss. Fig. 34 (a) shows larger contact area of T100-A than others which provides it higher COF.

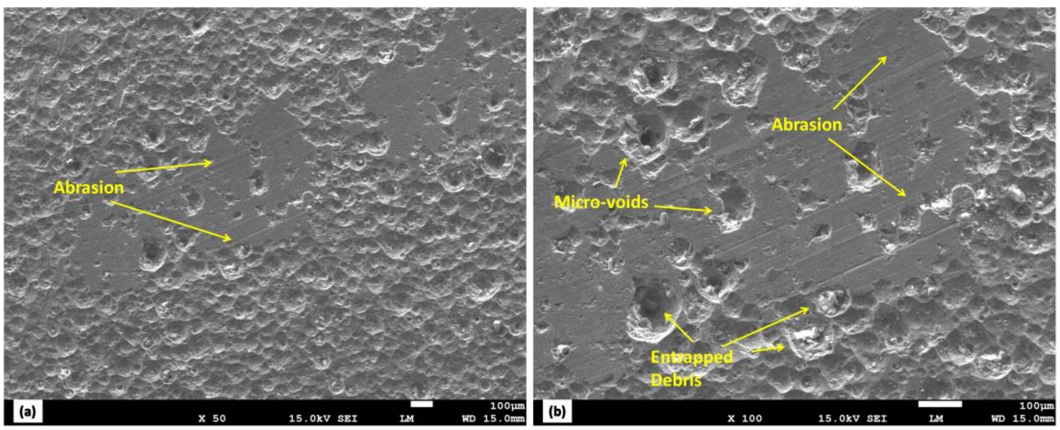

Fig. 35 SEM images of SMAT-A specimen - lubricated wear track.

Fig. 35 shows worn out surface of SMAT-A specimen. It clearly shows same wear mechanism like AH-A specimen. Mainly wear is due to abrasion of hard debris. It shows some micro-voids within wear track which may be due to either debris detachment or presence of porous Al_2O_3. These micro voids help in entrapment of wear debris which possibly helps to reduce its COF. Abrasive scratches are shallower and contact area is also lesser than other specimens which provide it lower volume loss. Lower wear loss for SMAT-A specimen is due to combined effect of Al_2O_3 coating and increased hardness due to SMAT.

Chapter 5

Conclusion

- Friction Stir Processing (FSP) was effectively used as solid state process of fabrication of Al 6060 aluminium composite using Zirconia as reinforcement. Grain refinement is observed in a stirred zone.
- FSPed specimen showed an increase in hardness. The hardness of AA-FSPZrO_2 specimen was more than that of AA-FSP specimen. Post-process age hardening (T6 heat treatment) resulted in further improvement in hardness which was twice that of AA specimen.
- Uniform texture patterns were generated on aluminium specimens using WEDM. WEDM texturing is found to be an effective method of texturing which can reduce COF in lubricated wear conditions. COF reduction is due to secondary lubrication provided by textured grooves.
- Shallower textures show less flattening than deeper textures which provide them lower wear loss.
- SMATed specimen showed the best results of improvement in hardness as well as tribological properties. COF reduction in lubricated condition is due to the combined effect of improved hardness as well as dimpled aluminium surface after SMAT.
- Successful anodizing of textured and SMATed specimen was carried out which provided them improved tribological properties.
- Hard anodized Al_2O_3 coating avoids direct aluminium to ball contact in initial stages which provide it lower wear loss than non-anodized specimens.
- Combination of SMAT and anodizing showed lowest wear loss in both dry and lubricated conditions due to presence of hard specimen surface as well as hard Al_2O_3 coating. In lubricated condition, AH-A specimen showed maximum reduction in COF up to 0.02 while SMAT and T50-A

specimen showed 0.03 COF. It is due to secondary lubrication provided by grooves and dimples.

- In case of lubricated condition, porous Al_2O_3 shows entrapment of wear debris which helps to reduce wear loss and COF. Moreover, oval shaped pores provide secondary lubrication which also promotes reduction in COF.
- Under dry condition, wear mechanism is mainly adhesive and abrasive. Adhesion, scuffing showed presence of adhesive wear while scratches, grooves, ploughing marks showed presence of abrasive wear.
- Non anodized specimens showed more adhesion which is due to lower hardness of specimen surface. Due to softening, non-anodized specimens have larger debris than anodized specimens. Instead of softening, harder wear debris in anodized specimens showed breaking.
- Wear mechanism for lubricated condition was mainly mild adhesive and abrasive. Non anodized textured specimens showed metal flow over grooves which increased their contact area and eventually increased COF. While, in case of anodized specimens, there was absence of metal flow which provided them better tribological properties.

Chapter 6

Future Scope

Aluminium alloys have bright future due to their increasing demand. Aluminium alloys are well known for their high strength and low weight. Due to these properties they are extensively used in aerospace and marine industries. In future aluminium alloys can be used in heavy duty manufacturing to reduce fuel consumption and improve performance. Countries like Japan are replacing railway bogies made up of steel with aluminium alloys. Researches can be further done to improve aluminium strength by alloying it with different elements. In future FSP can be used to make high strength alloys.

Automobile industries also have started use of aluminum alloys in making engine blocks and bearings which can provide better performance and wear resistance. Vehicle bodies can also be replaced by using aluminium alloys. Manufacturing cost will be more but it can be compensated by its performance. Research is going on biomedical applications of aluminium alloys where biocompatibility and tribological performance are major parameters. Surface texturing and SMAT can provide better tribological performance in future.

References

1. Meng, X., et al., *The Portevin-Le Chatelier effect of gradient nanostructured 5182 aluminum alloy by surface mechanical attrition treatment.* Journal of Materials Science & Technology, 2018. **34**(12): p. 2307-2315.
2. Denkena, B., J. Kästner, and B. Wang, *Advanced microstructures and its production through cutting and grinding.* CIRP annals, 2010. **59**(1): p. 67-72.
3. Dejun, K., W. Jinchun, and L. Hao, *Friction and wear performances of 7475 aluminium alloy after anodic oxidation.* Rare Metal Materials and Engineering, 2016. **45**(5): p. 1122-1127.
4. Rosochowski, A. *Processing metals by severe plastic deformation*. in *Solid State Phenomena*. 2005. Trans Tech Publ.
5. Kurt, A., I. Uygur, and E. Cete, *Surface modification of aluminium by friction stir processing.* Journal of materials processing technology, 2011. **211**(3): p. 313-317.
6. Kurt, H.I., *Influence of hybrid ratio and friction stir processing parameters on ultimate tensile strength of 5083 aluminum matrix hybrid composites.* Composites Part B: Engineering, 2016. **93**: p. 26-34.
7. Yuvaraj, N. and S. Aravindan, *Wear characteristics of Al5083 surface hybrid nano-composites by friction stir processing.* Transactions of the Indian Institute of Metals, 2017. **70**(4): p. 1111-1129.
8. Elangovan, K. and V. Balasubramanian, *Influences of pin profile and rotational speed of the tool on the formation of friction stir processing zone in AA2219 aluminium alloy.* Materials Science and Engineering: A, 2007. **459**(1-2): p. 7-18.

9. Prabhu, M.S., et al., *Friction and wear measurements of friction stir processed aluminium alloy 6082/CaCO3 composite.* Measurement, 2019. **142**: p. 10-20.
10. Deore, H., et al., *Effect of filler material and post process ageing treatment on microstructure, mechanical properties and wear behaviour of friction stir processed AA 7075 surface composites.* Surface and Coatings Technology, 2019. **374**: p. 52-64.
11. Mane, K.M. and S.S. Hosmani, *Friction Stir Surface Processing of Al 6061 Alloy: Role of Surface Alloying with Copper and Heat-Treatment.* Transactions of the Indian Institute of Metals, 2018. **71**(6): p. 1411-1425.
12. Ficici, F., *The experimental optimization of abrasive wear resistance model for an in-situ AlB2/Al-4Cu metal matrix composite.* Industrial Lubrication and Tribology, 2016. **68**(6): p. 632-639.
13. Kumar, M.P., et al., *Dry sliding wear behaviour of garnet particles reinforced zinc-aluminium alloy metal matrix composites.* Materials science, 2006. **12**(3): p. 209-213.
14. Krupka, I., P. Svoboda, and M. Hartl, *Effect of surface topography on mixed lubrication film formation during start up under rolling/sliding conditions.* Tribology International, 2010. **43**(5-6): p. 1035-1042.
15. Pettersson, U. and S. Jacobson, *Influence of surface texture on boundary lubricated sliding contacts.* Tribology International, 2003. **36**(11): p. 857-864.
16. Gatey, A., S. Hosmani, and R. Singh, *Surface mechanical attrition treated AISI 304L steel: role of process parameters.* Surface Engineering, 2016. **32**(1): p. 69-78.
17. Sun, Y. and R. Bailey, *Improvement in tribocorrosion behavior of 304 stainless steel by surface mechanical attrition treatment.* Surface and Coatings Technology, 2014. **253**: p. 284-291.
18. Liu, Y., B. Jin, and J. Lu, *Mechanical properties and thermal stability of nanocrystallized pure aluminum produced by surface mechanical attrition treatment.* Materials Science and Engineering: A, 2015. **636**: p. 446-451.

19. Chen, L., Z. Liu, and Q. Shen, *Enhancing tribological performance by anodizing micro-textured surfaces with nano-MoS2 coatings prepared on aluminum-silicon alloys.* Tribology International, 2018. **122**: p. 84-95.
20. Mirjavadi, S.S., et al., *Effect of multi-pass friction stir processing on the microstructure, mechanical and wear properties of AA5083/ZrO2 nanocomposites.* Journal of Alloys and Compounds, 2017. **726**: p. 1262-1273.
21. Gatey, A.M., et al. *Surface Engineering of Stainless Steels: Role of Surface Mechanical Attrition Treatment (SMAT)*. in *Advanced Materials Research*. 2013. Trans Tech Publ.
22. McNelley, T., S. Swaminathan, and J. Su, *Recrystallization mechanisms during friction stir welding/processing of aluminum alloys.* Scripta Materialia, 2008. **58**(5): p. 349-354.
23. Souza, P.H.L., C.A.S. de Oliveira, and J.M. do Vale Quaresma, *Precipitation hardening in dilute Al–Zr alloys.* Journal of materials research and technology, 2018. **7**(1): p. 66-72.
24. Rangaraju, N., et al., *Effect of cryo-rolling and annealing on microstructure and properties of commercially pure aluminium.* Materials Science and Engineering: A, 2005. **398**(1-2): p. 246-251.
25. Qian, H., et al., *Effects of Zr additive on microstructure, mechanical properties, and fractography of Al-Si Alloy.* Metals, 2018. **8**(2): p. 124.
26. Juyana, A.W. and M.N.B. Derman. *Characterization of porous anodic aluminium oxide film on aluminium templates formed in anodizing process*. in *Advanced Materials Research*. 2011. Trans Tech Publ.
27. Pettersson, U. and S. Jacobson, *Textured surfaces in sliding boundary lubricated contacts–mechanisms, possibilities and limitations.* Tribology-Materials, Surfaces & Interfaces, 2007. **1**(4): p. 181-189.
28. Al-Qutub, A., I. Allam, and T. Qureshi, *Effect of sub-micron Al2O3 concentration on dry wear properties of 6061 aluminum based composite.* Journal of Materials Processing Technology, 2006. **172**(3): p. 327-331.

29. Xavier, L.F. and P. Suresh, *Wear behavior of aluminium metal matrix composite prepared from industrial waste.* The Scientific World Journal, 2016. **2016**.
30. Arif, S., et al., *Characterization of surface morphology, wear performance and modelling of graphite reinforced aluminium hybrid composites.* Engineering Science and Technology, an International Journal, 2019.
31. Suryakumari, T. and S. Ranganathan, *Preparation and Study the Wear Behaviour of Aluminium Hybrid Composite.* Materials Today: Proceedings, 2018. **5**(2): p. 8104-8111.
32. SAXENA, A.K., *INVESTIGATION OF WEAR BEHAVIOR OF ALUMINIUM ALLOY AND COMPARISON WITH PURE ALUMINIUM*. 2012.
33. Gachot, C., et al., *A critical assessment of surface texturing for friction and wear improvement.* Wear, 2017. **372**: p. 21-41.
34. Spikes, H., *Mixed lubrication—an overview.* Lubrication Science, 1997. **9**(3): p. 221-253.
35. Costa, H. and I. Hutchings, *Effects of die surface patterning on lubrication in strip drawing.* Journal of Materials Processing Technology, 2009. **209**(3): p. 1175-1180.
36. Panagopoulos, C. and E. Georgiou, *Cold rolling and lubricated wear of 5083 aluminium alloy.* Materials & Design, 2010. **31**(3): p. 1050-1055.
37. Ranjan, R., et al., *Laser texturing for low-flying-height media.* Journal of Applied Physics, 1991. **69**(8): p. 5745-5747.
38. Lu, P., et al., *The use of anisotropic texturing for control of directional friction.* Tribology International, 2017. **113**: p. 169-181.
39. Iwai, Y., et al., *Wear behaviour of high tensile strength aluminium alloys under dry and lubricated conditions.* Wear, 1996. **196**(1-2): p. 46-53.
40. Bermudez, M., et al., *Dry and lubricated wear resistance of mechanically-alloyed aluminium-base sintered composites.* Wear, 2001. **248**(1-2): p. 178-186.